

Auxiliary field diffusion Monte Carlo calculations of light- and medium-mass nuclei with local chiral interactions

D. Lonardoni,^{1,2} S. Gandolfi,² J. Carlson,² C. Petrie,³ K. E. Schmidt,³ J. E. Lynn,^{4,5} and A. Schwenk^{4,5,6}

¹*National Superconducting Cyclotron Laboratory, Michigan State University, East Lansing, Michigan 48824, USA*

²*Theoretical Division, Los Alamos National Laboratory, Los Alamos, New Mexico 87545, USA*

³*Department of Physics, Arizona State University, Tempe, Arizona 85287, USA*

⁴*Institut für Kernphysik, Technische Universität Darmstadt, 64289 Darmstadt, Germany*

⁵*ExtreMe Matter Institute EMMI, GSI Helmholtzzentrum für Schwerionenforschung GmbH, 64291 Darmstadt, Germany*

⁶*Max-Planck-Institut für Kernphysik, Saupfercheckweg 1, 69117 Heidelberg, Germany*

Quantum Monte Carlo methods have been recently employed to study properties of nuclei and infinite matter using local chiral effective field theory interactions. In this work, we present a detailed description of the auxiliary field diffusion Monte Carlo algorithm for nuclei in combination with local chiral two- and three-nucleon forces up to next-to-next-to-leading order. We show results for the binding energy, charge radius, charge form factor, and Coulomb sum rule in nuclei with $3 \leq A \leq 16$. Particular attention is devoted to the effect of different operator structures in the three-body force for different cutoffs. The outcomes suggest that harder interactions fit to few-body observables give a very good description of the ground state properties of nuclei up to ^{16}O . Softer interactions manifest instead a significant dependence on the employed operator structure and possibly call for the necessity of inputs other than few-body observables.

I. INTRODUCTION

The solution of the many-body Schrödinger equation describing a system of individual interacting baryons is challenging because of the non-perturbative nature and the strong spin-isospin dependence of realistic nuclear interactions. Quantum Monte Carlo (QMC) methods provide a powerful tool to tackle the nuclear many-body problem in a non-perturbative fashion. They have been proven to be remarkably successful in describing the properties of strongly correlated Fermions in a large variety of physical conditions [1].

Historically, QMC methods have made use of phenomenological nuclear interactions, such as the Argonne v_{18} (AV18) nucleon-nucleon potential combined with Urbana/Illinois models for the three-body forces [1]. By construction, these potentials are nearly local, meaning that the dominant parts of the interaction depend only on the relative distance, spin, and isospin of the two interacting nucleons, and not upon their momenta. This feature has been one of the keys to success for the application of QMC algorithms to the study of nuclear systems. Green's function Monte Carlo (GFMC) and auxiliary field diffusion Monte Carlo (AFDMC) have been employed to derive properties of nuclei, neutron drops, and neutron star matter [2–8]. Despite the large success of such models, phenomenological interactions are not free of drawbacks. They do not provide a systematic way to estimate theoretical uncertainties, and it is not clear how to improve their quality. In addition, some models of the three-body force provide a too soft equation of state of neutron matter [4, 9], with the consequence that the predicted neutron star maximum mass is not compatible with the observation of heavy neutron stars [10, 11].

An alternative approach to nuclear interactions that overcomes the limitations of the phenomenological mod-

els is provided by chiral effective field theory (EFT) [12, 13]. In chiral EFT nuclear interactions are systematically derived accordingly with the underlying theory of the strong interaction. The most general Lagrangian consistent with the symmetries of low-energy quantum chromodynamics (QCD) is written in terms of the relevant degrees of freedom at low energies, i.e., nucleons and pions. A power counting scheme is then chosen to order the resulting contributions according to their importance. The result is a low-energy effective field theory according to which the nuclear interaction is written as an expansion on the ratio of a soft scale (the pion mass or a typical momentum scale in the nucleus) to a hard scale (the chiral breakdown scale). The long-range part of the potential is given by pion-exchange contributions, that are determined by the chiral symmetry of QCD and low-energy experimental data for the pion-nucleon system. The short-range terms are instead characterized by contact interactions described by the so-called low-energy constants (LECs), that are fit to reproduce experimental data (nucleon-nucleon scattering data for the two-body part of the interaction, and few- and/or many-body observables for the many-body components). Among the advantages of such an expansion compared to traditional approaches, are the ability of systematically improve the quality of the interaction order by order, the possibility of estimate theoretical uncertainties, the fact that many-body forces arise naturally, and that electroweak currents can be derived consistently.

In the last decade intense effort has been devoted to the development of chiral EFT interactions, as testified by the availability of different potential models in the literature [12–18], typically written in momentum space. It is only in recent years that chiral EFT interactions have been equivalently formulated in coordinate space. New potentials are now available, including next-to-next-to-leading-order (N²LO) local forces [19, 20], supported by

consistent three-body potentials [21, 22], as well as chiral interactions with explicit delta degrees of freedom [18, 23–25].

The local version of chiral forces can be written using the same operator structure as the phenomenological potentials, providing for the first time the opportunity to combine EFT derived interactions and exact QMC methods. GFMC has been used to study the ground state of light nuclei employing the local chiral forces [19–22, 26]. The same potentials have been used in AFDMC calculations of pure neutron systems, ranging from few-body systems [27–30], to pure neutron matter [19–21]. More recently, the first AFDMC study of p -shell nuclei employing local chiral forces has been reported [31]. In this work we provide a comprehensive description of the AFDMC algorithm for the study of ground state properties of light- and medium-mass nuclei employing the local version of chiral interactions at N²LO, extending the findings of Ref. [31].

The structure of this paper is as follows. In Section II we introduce the nuclear Hamiltonian employed in this work. In Sections III and IV we review the main features of the VMC and AFDMC methods. Section V is devoted to the description of the employed wave function. In Section VI we present a collection of results for nuclei with $3 \leq A \leq 16$. Finally, we give a summary in Section VII.

II. HAMILTONIAN

Nuclei are described as a collection of point-like particles of mass m_N interacting via two- and three-body forces accordingly to the nonrelativistic Hamiltonian

$$H = -\frac{\hbar^2}{2m_N} \sum_i \nabla_i^2 + \sum_{i<j} v_{ij} + \sum_{i<j<k} V_{ijk}, \quad (1)$$

where the two-body interaction v_{ij} also includes the Coulomb force.

In QMC calculations it is convenient to express the interactions in terms of radial functions multiplying spin and isospin operators. The commonly employed Argonne v'_8 (AV8') potential [32], as well as the two-body part of the recently developed chiral interactions in local form [19], can be expressed as:

$$v_{ij} = \sum_{p=1}^8 v_p(r_{ij}) \mathcal{O}_{ij}^p, \quad (2)$$

with

$$\mathcal{O}_{ij}^{p=1,8} = [\mathbb{1}, \boldsymbol{\sigma}_i \cdot \boldsymbol{\sigma}_j, S_{ij}, \mathbf{L} \cdot \mathbf{S}] \otimes [\mathbb{1}, \boldsymbol{\tau}_i \cdot \boldsymbol{\tau}_j], \quad (3)$$

where

$$S_{ij} = 3 \boldsymbol{\sigma}_i \cdot \hat{\mathbf{r}}_{ij} \boldsymbol{\sigma}_j \cdot \hat{\mathbf{r}}_{ij} - \boldsymbol{\sigma}_i \cdot \boldsymbol{\sigma}_j, \quad (4)$$

is the tensor operator, and

$$\mathbf{L} = \frac{1}{2i} (\mathbf{r}_i - \mathbf{r}_j) \times (\nabla_i - \nabla_j), \quad (5)$$

$$\mathbf{S} = \frac{1}{2} (\boldsymbol{\sigma}_i + \boldsymbol{\sigma}_j), \quad (6)$$

\mathbf{L} and \mathbf{S} being the relative angular momentum and the total spin of the pair ij , respectively. The radial functions of Eq. (2) are fitted to nucleon-nucleon scattering data. At N²LO, the operator structure of the local chiral interactions is the same as above, with the only exception for the missing $\mathbf{L} \cdot \mathbf{S} \boldsymbol{\tau}_i \cdot \boldsymbol{\tau}_j$ term (see Ref. [20] for more details).

The three-body force V_{ijk} is written as a sum of contributions coming from two-pion exchange (TPE), plus short range terms. In the case of local chiral forces at N²LO, P - and S -wave TPE contributions are included, and they are characterized by the same LECs involved in the two-body sector. The short range part of the three-body force is instead parametrized by two contact terms, the LECs of which have been fit to the alpha particle binding energy and to the spin-orbit splitting in the neutron- α P -wave phase shifts (see Refs. [22, 26] for more details).

The chiral three-body interaction at N²LO can be conveniently written as

$$V = V_a^{2\pi,P} + V_c^{2\pi,P} + V^{2\pi,S} + V_D + V_E, \quad (7)$$

where the first three terms correspond to the TPE diagrams in P and S waves (Eqs. (A.1b), (A.1c) and (A.1a) of Ref. [26], respectively). The subscripts a and c refer to the operator structure of such contributions, that can be written in terms of anticommutators or commutators, respectively. V_D and V_E involve contact terms. In this work we employ the form (A.2b) of Ref. [26] for V_D , and we consider two choices for V_E , namely $E\tau$ and $E1$ (Eqs. (A.3a) and (A.3b) of Ref. [26]).

By defining the following quantities:

$$\begin{aligned} \delta_{R_0}(r) &= \frac{n}{4\pi R_0^3 \Gamma(3/n)} e^{-(r/R_0)^n}, \\ T(r) &= \left(1 + \frac{3}{m_\pi r} + \frac{9}{m_\pi^2 r^2}\right) \frac{e^{-m_\pi r}}{m_\pi r} T_c(r), \\ Y(r) &= \frac{e^{-m_\pi r}}{m_\pi r} Y_c(r), \\ Z(r) &= \frac{m_\pi r}{3} (Y(r) - T(r)), \\ Y_c(r) &= 1 - e^{-(r/R_0)^n}, \\ T_c(r) &= \left(1 - e^{-(r/R_0)^n}\right)^{nt}, \\ X_{i\alpha j\beta} &= (3 \hat{\mathbf{x}}_\alpha \cdot \hat{\mathbf{r}}_{ij} \hat{\mathbf{x}}_\beta \cdot \hat{\mathbf{r}}_{ij} - \delta_{\alpha\beta}) T(r_{ij}) + \delta_{\alpha\beta} Y(r_{ij}), \\ \mathcal{X}_{i\alpha j\beta} &= X_{i\alpha j\beta}(\mathbf{r}_{ij}) - \delta_{\alpha\beta} \frac{4\pi}{m_\pi^3} \delta_{R_0}(r_{ij}), \\ \mathcal{Z}_{i\alpha} &= Z(r_{ij}) \hat{\mathbf{x}}_\alpha \cdot \hat{\mathbf{r}}_{ij}, \end{aligned} \quad (8)$$

we can recast the contributions of Eq. (7) in a form that is suitable for QMC calculations:

$$\begin{aligned}
V_a^{2\pi,P} &= A_a^{2\pi,P} \sum_{i<j<k} \sum_{cyc} \left\{ \boldsymbol{\tau}_i \cdot \boldsymbol{\tau}_k, \boldsymbol{\tau}_j \cdot \boldsymbol{\tau}_k \right\} \left\{ \sigma_i^\alpha \sigma_k^\gamma, \sigma_k^\mu \sigma_j^\beta \right\} \mathcal{X}_{i\alpha k\gamma} \mathcal{X}_{k\mu j\beta} \\
&= 4 A_a^{2\pi,P} \sum_{i<j} \boldsymbol{\tau}_i \cdot \boldsymbol{\tau}_j \sigma_i^\alpha \sigma_j^\beta \sum_{k \neq i,j} \mathcal{X}_{i\alpha k\gamma} \mathcal{X}_{k\mu j\beta} \\
&= 4 A_a^{2\pi,P} \sum_{i<j} \boldsymbol{\tau}_i \cdot \boldsymbol{\tau}_j \sigma_i^\alpha \sigma_j^\beta \sum_{k \neq i,j} \left(X_{i\alpha k\gamma} - \delta_{\alpha\gamma} \frac{4\pi}{m_\pi^3} \delta_{R_0}(r_{ik}) \right) \left(X_{k\mu j\beta} - \delta_{\mu\beta} \frac{4\pi}{m_\pi^3} \delta_{R_0}(r_{kj}) \right) \\
&= V_a^{XX} + V_a^{X\delta} + V_a^{\delta\delta}, \tag{9}
\end{aligned}$$

$$\begin{aligned}
V_c^{2\pi,P} &= A_c^{2\pi,P} \sum_{i<j<k} \sum_{cyc} \left[\boldsymbol{\tau}_i \cdot \boldsymbol{\tau}_k, \boldsymbol{\tau}_j \cdot \boldsymbol{\tau}_k \right] \left[\sigma_i^\alpha \sigma_k^\gamma, \sigma_k^\mu \sigma_j^\beta \right] \mathcal{X}_{i\alpha k\gamma} \mathcal{X}_{k\mu j\beta} \\
&= -4 A_c^{2\pi,P} \sum_{i<j<k} \sum_{cyc} \tau_i^\eta \tau_j^\xi \tau_k^\phi \epsilon_{\eta\xi\phi} \sigma_i^\alpha \sigma_j^\beta \sigma_k^\nu \epsilon_{\nu\gamma\mu} \mathcal{X}_{i\alpha k\gamma} \mathcal{X}_{k\mu j\beta} \\
&= A_c^{2\pi,P} \sum_{i<j<k} \sum_{cyc} \left[\boldsymbol{\tau}_i \cdot \boldsymbol{\tau}_k, \boldsymbol{\tau}_j \cdot \boldsymbol{\tau}_k \right] \left[\sigma_i^\alpha \sigma_k^\gamma, \sigma_k^\mu \sigma_j^\beta \right] \left(X_{i\alpha k\gamma} - \delta_{\alpha\gamma} \frac{4\pi}{m_\pi^3} \delta_{R_0}(r_{ik}) \right) \left(X_{k\mu j\beta} - \delta_{\mu\beta} \frac{4\pi}{m_\pi^3} \delta_{R_0}(r_{kj}) \right) \\
&= V_c^{XX} + V_c^{X\delta} + V_c^{\delta\delta}, \tag{10}
\end{aligned}$$

$$\begin{aligned}
V^{2\pi,S} &= A^{2\pi,S} \sum_{i<j<k} \sum_{cyc} \boldsymbol{\tau}_i \cdot \boldsymbol{\tau}_j \sigma_i^\alpha \sigma_j^\beta \mathcal{Z}_{ik\alpha} \mathcal{Z}_{jk\alpha} \\
&= A^{2\pi,S} \sum_{i<j} \boldsymbol{\tau}_i \cdot \boldsymbol{\tau}_j \sigma_i^\alpha \sigma_j^\beta \sum_{k \neq i,j} \mathcal{Z}_{ik\alpha} \mathcal{Z}_{jk\alpha}, \tag{11}
\end{aligned}$$

$$\begin{aligned}
V_D &= A_D \sum_{i<j} \boldsymbol{\tau}_i \cdot \boldsymbol{\tau}_j \sigma_i^\alpha \sigma_j^\beta \sum_{k \neq i,j} \mathcal{X}_{i\alpha j\beta} \left[\delta_{R_0}(r_{ik}) + \delta_{R_0}(r_{jk}) \right], \\
&= A_D \sum_{i<j} \boldsymbol{\tau}_i \cdot \boldsymbol{\tau}_j \sigma_i^\alpha \sigma_j^\beta \sum_{k \neq i,j} \left(X_{i\alpha j\beta} - \delta_{\alpha\beta} \frac{4\pi}{m_\pi^3} \delta_{R_0}(r_{ij}) \right) \left[\delta_{R_0}(r_{ik}) + \delta_{R_0}(r_{jk}) \right], \\
&= V_D^{X\delta} + V_D^{\delta\delta} \tag{12}
\end{aligned}$$

$$V_E = A_E \sum_{i<j} \boldsymbol{\tau}_i \cdot \boldsymbol{\tau}_j \sum_{k \neq i,j} \delta_{R_0}(r_{ik}) \delta_{R_0}(r_{jk}), \tag{13}$$

where the sum over the coordinate projections (Greek letter indexes) is implicit. Equation (13) is the expression for the $E\tau$ parametrization of the contact term V_E . The $E1$ form is recovered setting $\boldsymbol{\tau}_i \cdot \boldsymbol{\tau}_j = 1$. For the local chiral interactions at N²LO, we have

$$\begin{aligned}
A_a^{2\pi,P} &= \frac{1}{2} \left(\frac{g_A}{f_\pi^2} \right)^2 \left(\frac{1}{4\pi} \right)^2 \frac{m_\pi^6}{9} c_3, \\
A_c^{2\pi,P} &= -\frac{c_4}{2c_3} A_a^{2\pi,P}, \\
A^{2\pi,S} &= \left(\frac{g_A}{2f_\pi} \right)^2 \left(\frac{m_\pi}{4\pi} \right)^2 \frac{4m_\pi^6}{f_\pi^2} c_1, \\
A_D &= \frac{m_\pi^3}{12\pi} \frac{g_A}{8f_\pi^2} \frac{1}{f_\pi^2 \Lambda_\chi} c_D, \\
A_E &= \frac{c_E}{f_\pi^4 \Lambda_\chi}. \tag{14}
\end{aligned}$$

Note that, using these definitions, the structure of the phenomenological Urbana IX (UIX) model is recovered by imposing $\delta_{R_0}(r) = 0$, $n = 2$, $n_t = 2$, and $A_c^{2\pi,P} =$

$$\frac{1}{4} A_a^{2\pi,P}.$$

III. REVIEW OF VMC

In variational Monte Carlo (VMC), given a trial wave function Ψ_T , the expectation value of the Hamiltonian H is given by

$$E_0 \leq \langle H \rangle = \frac{\langle \Psi_T | H | \Psi_T \rangle}{\langle \Psi_T | \Psi_T \rangle} = \frac{\int dR \Psi_T^*(R) H \Psi_T(R)}{\int dR \Psi_T^*(R) \Psi_T(R)}, \tag{15}$$

where $R = \{\mathbf{r}_1, \dots, \mathbf{r}_A\}$ are the coordinates of the particles, and there is an implicit sum over all the particle spin and isospin states. E_0 is the energy of the true ground-state with the same quantum numbers as Ψ_T , and the equality in the above relation is valid only if the wave function is the exact ground state wave function Ψ_0 . In VMC one typically minimizes the energy expectation value of Eq. (15) with respect to changes in the

variational parameters, in order to obtain Ψ_T as close as possible to Ψ_0 .

The integral of Eq. (15) can be rewritten as

$$\langle H \rangle = \frac{\int dR P(R) \frac{H\Psi_T(R)}{\Psi_T(R)}}{\int dR P(R)}, \quad (16)$$

where $P(R) = |\Psi_T(R)|^2$ can be interpreted as a probability distribution of points R in a 3A dimensional space. The above multi-dimensional integral can be solved using Monte Carlo sampling. In practice, a number of configurations R_i are sampled using the Metropolis algorithm [33], and the local energy of the system is calculated as:

$$\langle E \rangle = \frac{1}{A} \sum_{i=1}^A \frac{\langle R_i | H | \Psi_T \rangle}{\langle R_i | \Psi_T \rangle}, \quad (17)$$

where $\langle R | \Psi_T \rangle = \Psi_T(R)$. More details on the sampling procedure and on the calculation of statistical errors can be found for example in Ref. [34].

For spin/isospin dependent interactions the generalization of Eq. (15) is straightforward:

$$\langle H \rangle = \frac{\int dR \sum_{S,S'} \Psi_T^*(R, S') H_{S,S'} \Psi_T(R, S)}{\int dR \sum_S |\Psi_T(R, S)|^2}, \quad (18)$$

where now the wave function also depends upon spin and isospin states $S = \{s_1, \dots, s_A\}$, and

$$H_{S,S'} = \langle S' | S \rangle \left[-\frac{\hbar^2}{2m} \sum_i \nabla_i^2 \right] + \langle RS' | V | RS \rangle. \quad (19)$$

In this case, VMC can be implemented with either explicit sum over all the spins/isospin states

$$\begin{aligned} \langle H \rangle &= \int dR E_L(R) P(R), \\ P(R) &= \frac{\sum_S |\Psi_T(R, S)|^2}{\int dR \sum_S |\Psi_T(R, S)|^2}, \\ E_L(R) &= \frac{\sum_{S,S'} \Psi_T^*(R, S') H_{S,S'} \Psi_T(R, S)}{\sum_S |\Psi_T(R, S)|^2}, \end{aligned} \quad (20)$$

or with spin/isospin samples:

$$\begin{aligned} \langle H \rangle &= \int dR \sum_S E_L(R, S) P(R, S), \\ P(R, S) &= \frac{|\Psi_T(R, S)|^2}{\int dR |\Psi_T(R, S)|^2}, \\ E_L(R, S) &= \frac{\sum_{S'} \Psi_T^*(R, S') H_{S,S'} \Psi_T(R, S)}{|\Psi_T(R, S)|^2}. \end{aligned} \quad (21)$$

The Metropolis algorithm can be then used to sample either R from $P(R)$ in the first case, or R and S from $P(R, S)$ in the latter case.

IV. REVIEW OF AFDMC

Diffusion Monte Carlo (DMC) methods are used to project out the ground state with a particular set of quantum numbers. The starting point is a trial wave function $|\Psi_T\rangle$, typically the result of a VMC minimization, that is propagated in imaginary time τ :

$$|\Psi_0\rangle \propto \lim_{\tau \rightarrow \infty} e^{-(H-E_T)\tau} |\Psi_T\rangle, \quad (22)$$

where H is the Hamiltonian describing the system, and E_T is a parameter that controls the normalization. For spin/isospin independent interactions, the object to be propagated is given by the overlap between the wave function and a set of configurations in coordinate space $\langle R | \Psi_T \rangle = \Psi_T(R)$. By using the completeness relation $\int dR |R\rangle \langle R| = \mathbb{1}$, we can write the propagation in imaginary time as

$$\langle R' | \Psi(\tau) \rangle = \int dR G(R', R, \tau) \langle R | \Psi_T(0) \rangle, \quad (23)$$

where the propagator (or Green's function) G is defined as the matrix element between the two points R and R' in the volume

$$G(R', R, \tau) = \langle R' | e^{-(H-E_T)\tau} | R \rangle, \quad (24)$$

and $\langle R' | \Psi(\tau) \rangle$ approaches the true ground-state for large imaginary time.

In practice, it is not possible to directly compute the propagator $G(R', R, \tau)$. However, one can use the short-time propagator $G(R', R, d\tau)$:

$$\begin{aligned} \langle R' | \Psi(\tau) \rangle &= \int dR_n dR_{n-1} \dots dR_1 dR G(R', R_n, \delta\tau) \times \\ &\quad \times G(R_{n-1}, R_{n-2}, \delta\tau) \dots G(R_1, R, \delta\tau) \langle R | \Psi_T(0) \rangle, \end{aligned} \quad (25)$$

and then employ Monte Carlo techniques to sample the paths R_i in the imaginary time evolution. The method is accurate for small values of the time step $\delta\tau$, and the exact result can be determined by using different values of $\delta\tau$ and extrapolating for $\delta\tau \rightarrow 0$.

By using the Trotter-Suzuki relation to order $d\tau^3$, the short-time propagator can be approximated with:

$$\begin{aligned} G(R', R, \delta\tau) &\equiv \langle R' | e^{-(H-E_T)\delta\tau} | R \rangle \\ &\approx \langle R' | e^{-(V-E_T)\frac{\delta\tau}{2}} e^{-T\delta\tau} e^{-(V-E_T)\frac{\delta\tau}{2}} | R \rangle, \end{aligned} \quad (26)$$

where T is the non-relativistic kinetic energy, and V is the employed potential. The propagator for the kinetic

energy alone corresponds to the free particle propagator:

$$G_0(R', R) = \langle R' | e^{-T\delta\tau} | R \rangle = \left(\frac{m}{2\pi\hbar^2\delta\tau} \right)^{\frac{3A}{2}} e^{-\frac{m(R-R')^2}{2\hbar^2\delta\tau}}, \quad (27)$$

that yields a Gaussian diffusion for the paths in coordinate space, with $\sigma^2 = 4\frac{\hbar^2}{2m}\delta\tau$. The propagator for spin/isospin independent potentials is simply given by:

$$\langle R' | e^{-(V-E_T)\delta\tau} | R \rangle \approx \prod_{i<j} e^{-[V(r_{ij})-E_T]\delta\tau} \delta_{R'R}, \quad (28)$$

where, each pair interaction can be simply evaluated as a function of the coordinates of the system, and the energy E_T results in a normalization factor. Note that the addition of spin/isospin independent three- and many-body interactions is straightforward.

For spin/isospin dependent interactions, the propagation of the potential becomes more complicated. In general, this is because quadratic operators like $\sigma_i \cdot \sigma_j$ generates amplitudes along the singlet and the triplet states of a pair. The propagator (28) generalizes in this case to

$$\begin{aligned} \langle R' | e^{-(V-E_T)\delta\tau} | R \rangle &\rightarrow \langle R' S' | e^{-(V-E_T)\delta\tau} | R S \rangle \\ &\approx \langle S' | \prod_{i<j} e^{-(V(r_{ij})-E_T)\delta\tau} | S \rangle \delta_{RR'}, \end{aligned} \quad (29)$$

where now the matrix $\exp[-(V-E_T)\delta\tau]$ is not diagonal in the spin of each pair. One possible strategy to compute the propagator (29) is to include all the spin/isospin states in the trial wave function, as done in GFMC [1]. This, however, implies a number of wave function components proportional to 2^A , that currently limits GFMC calculations to $A = 12$.

The idea of auxiliary field diffusion Monte Carlo is to start from a trial wave function whose computational cost is polynomial with A , rather than exponential. Such a wave function can be written in the single particle representation:

$$\langle S | \Psi \rangle \propto \xi_{\alpha_1}(s_1) \xi_{\alpha_2}(s_2) \dots \xi_{\alpha_A}(s_A), \quad (30)$$

where $\xi_{\alpha_i}(s_i)$ are functions of the spinor s_i with state α_i . In the above expression, the radial orbitals are omitted for simplicity, and the antisymmetrization is trivial.

A quadratic operator in the spin acting on the wave function above generates two different amplitudes:

$$\begin{aligned} \langle S | \sigma_1 \cdot \sigma_2 | \Psi \rangle &= \langle S | 2\mathcal{P}_{12}^\sigma - \mathbb{1} | \Psi \rangle \\ &= 2\xi_{\alpha_1}(s_2) \xi_{\alpha_2}(s_1) \xi_{\alpha_3}(s_3) \dots \xi_{\alpha_A}(s_A) \\ &\quad - \xi_{\alpha_1}(s_1) \xi_{\alpha_2}(s_2) \xi_{\alpha_3}(s_3) \dots \xi_{\alpha_A}(s_A) \\ &= \langle S' | \Psi \rangle + \langle S'' | \Psi \rangle. \end{aligned} \quad (31)$$

In general, the action of all pairwise spin/isospin operators (or propagators) generates $2^A \binom{A}{Z}$ amplitudes (if charge conservation is imposed). Even though this number can be further reduced by assuming that the nucleus has good isospin [1], the action of pairwise operators largely increases the number of components with respect to the initial wave function, losing thus the computational advantage of the polynomial scaling with A . However, linear spin/isospin operators do not break the single particle representation. They simply imply rotations of the initial spinors, without generating new amplitudes, as for instance:

$$\begin{aligned} \langle S | \sigma_1^\alpha | \Psi \rangle &= \sigma_1^\alpha \xi_{\alpha_1}(s_1) \xi_{\alpha_2}(s_2) \xi_{\alpha_3}(s_3) \dots \xi_{\alpha_A}(s_A) \\ &= \xi_{\alpha_1}(s'_1) \xi_{\alpha_2}(s_2) \xi_{\alpha_3}(s_3) \dots \xi_{\alpha_A}(s_A) \\ &= \langle S' | \Psi \rangle. \end{aligned} \quad (32)$$

Quadratic operators can be linearized by using the Hubbard-Stratonovich transformation:

$$e^{-\frac{1}{2}\lambda\mathcal{O}^2} = \frac{1}{\sqrt{2\pi}} \int dx e^{-\frac{x^2}{2} + \sqrt{-\lambda}x\mathcal{O}}, \quad (33)$$

where x are usually called *auxiliary fields*, and the integral above can be computed with Monte Carlo techniques, i.e. by sampling points x with probability distribution $P(x) = \exp(-x^2/2)$. By using the transformation (33), Hamiltonians involving up to quadratic operators in spin and isospin can be efficiently employed in the imaginary time propagation of a trial wave function of the form (30), retaining the good polynomial scaling with A .

A. Propagation of spin/isospin quadratic operators

Let's consider the two-body interaction of Eq. (2) up to $p = 6$:

$$\begin{aligned}
V_{NN}^6 &= \sum_{i < j} \left\{ \left[v_1(r_{ij}) + v_2(r_{ij}) \boldsymbol{\tau}_i \cdot \boldsymbol{\tau}_j \right] \mathbb{1} + \left[v_3(r_{ij}) + v_4(r_{ij}) \boldsymbol{\tau}_i \cdot \boldsymbol{\tau}_j \right] \boldsymbol{\sigma}_i \cdot \boldsymbol{\sigma}_j + \left[v_5(r_{ij}) + v_6(r_{ij}) \boldsymbol{\tau}_i \cdot \boldsymbol{\tau}_j \right] S_{ij} \right\}, \\
&= \sum_{i < j} v_1(r_{ij}) + \sum_{i < j} \left[v_2(r_{ij}) \right] \boldsymbol{\tau}_i \cdot \boldsymbol{\tau}_j + \sum_{i < j} \sum_{\alpha\beta} \left[v_3(r_{ij}) \delta_{\alpha\beta} + v_5(r_{ij}) (3 \hat{r}_{ij}^\alpha \hat{r}_{ij}^\beta - \delta_{\alpha\beta}) \right] \sigma_i^\alpha \sigma_j^\beta \\
&\quad + \sum_{i < j} \sum_{\alpha\beta} \left[v_4(r_{ij}) \delta_{\alpha\beta} + v_6(r_{ij}) (3 \hat{r}_{ij}^\alpha \hat{r}_{ij}^\beta - \delta_{\alpha\beta}) \right] \boldsymbol{\tau}_i \cdot \boldsymbol{\tau}_j \sigma_i^\alpha \sigma_j^\beta, \\
&= V_{SI}(R) + \frac{1}{2} \sum_{i \neq j} A_{ij}^{(\tau)} \boldsymbol{\tau}_i \cdot \boldsymbol{\tau}_j + \frac{1}{2} \sum_{i \neq j} \sum_{\alpha\beta} A_{i\alpha j\beta}^{(\sigma)} \sigma_i^\alpha \sigma_j^\beta + \frac{1}{2} \sum_{i \neq j} \sum_{\alpha\beta} A_{i\alpha j\beta}^{(\sigma\tau)} \boldsymbol{\tau}_i \cdot \boldsymbol{\tau}_j \sigma_i^\alpha \sigma_j^\beta, \\
&= V_{SI}(R) + V_{SD}
\end{aligned} \tag{34}$$

where $V_{SI}(V_{SD})$ is the spin/isospin-independent(-dependent) part of the interaction, and $A_{ij}^{(\tau)}$ ($A \times A$), $A_{i\alpha j\beta}^{(\sigma)}$ ($3A \times 3A$), and $A_{i\alpha j\beta}^{(\sigma\tau)}$ ($3A \times 3A$) are real and symmetric matrices. As such, these matrices can be diagonalized:

$$\begin{aligned}
\sum_j A_{ij}^{(\tau)} \psi_{n,j}^{(\tau)} &= \lambda_n^{(\tau)} \psi_{n,i}^{(\tau)}, \\
\sum_{j\beta} A_{i\alpha j\beta}^{(\sigma)} \psi_{n,j\beta}^{(\sigma)} &= \lambda_n^{(\sigma)} \psi_{n,i\alpha}^{(\sigma)}, \\
\sum_{j\beta} A_{i\alpha j\beta}^{(\sigma\tau)} \psi_{n,j\beta}^{(\sigma\tau)} &= \lambda_n^{(\sigma\tau)} \psi_{n,i\alpha}^{(\sigma\tau)},
\end{aligned} \tag{35}$$

and it is possible to define a new set of operators expressed in terms of their eigenvectors:

$$\begin{aligned}
\mathcal{O}_{n\alpha}^{(\tau)} &= \sum_j \tau_j^\alpha \psi_{n,j}^{(\tau)}, \\
\mathcal{O}_n^{(\sigma)} &= \sum_{j\beta} \sigma_j^\beta \psi_{n,j\beta}^{(\sigma)}, \\
\mathcal{O}_{n\alpha}^{(\sigma\tau)} &= \sum_{j\beta} \tau_j^\alpha \sigma_j^\beta \psi_{n,j\beta}^{(\sigma\tau)},
\end{aligned} \tag{36}$$

such that the spin/isospin-dependent part of Eq. (34) can be recast as:

$$\begin{aligned}
V_{SD} &= \frac{1}{2} \sum_{\alpha=1}^3 \sum_{n=1}^A \lambda_n^{(\tau)} \left(\mathcal{O}_{n\alpha}^{(\tau)} \right)^2 + \frac{1}{2} \sum_{n=1}^{3A} \lambda_n^{(\sigma)} \left(\mathcal{O}_n^{(\sigma)} \right)^2 \\
&\quad + \frac{1}{2} \sum_{\alpha=1}^3 \sum_{n=1}^{3A} \lambda_n^{(\sigma\tau)} \left(\mathcal{O}_{n\alpha}^{(\sigma\tau)} \right)^2.
\end{aligned} \tag{37}$$

The potential written in this form contains only quadratic operators in spin/isospin. We can thus use the Hubbard-Stratonovich transformation (33) to write the propagator of the V_{NN}^6 interaction acting on a configuration $|RS\rangle$ as:

$$e^{-V_{NN}^6 \delta\tau} |RS\rangle = e^{-V_{SI}(R) \delta\tau} \prod_{m=1}^{15A} \frac{1}{\sqrt{2\pi}} \int dx_m e^{\frac{x_m^2}{2}} e^{\sqrt{-\lambda_m \delta\tau} x_m \mathcal{O}_m} |RS\rangle = |RS'\rangle, \tag{38}$$

where 15 auxiliary fields are needed for each nucleon, 3 for τ operators, 3 for σ , and 9 for $\sigma\tau$. The propagation (rotation) of spinors depends upon the sampling of the auxiliary fields $X = \{x_m\}$, so as the new spin/isospin

configurations S' , that, for this reason, will be indicated as $S'(X)$. The full short-time propagator, that includes both kinetic energy and potential, can be finally expressed as:

$$G(R', R, S', S, \delta\tau) = \langle R' S' | \left(\frac{m}{2\pi\hbar^2\delta\tau} \right)^{\frac{3A}{2}} e^{-\frac{m(R-R')^2}{2\hbar^2\delta\tau}} e^{-(V_{SI}(R)-E_T)\delta\tau} \prod_{m=1}^{15A} \frac{1}{\sqrt{2\pi}} \int dx_m e^{-\frac{x_m^2}{2}} e^{\sqrt{-\lambda_m\delta\tau} x_m \mathcal{O}_m} |RS\rangle, \quad (39)$$

Note that the above expressions refer to the simple propagator $\exp[-T\delta\tau]\exp[-(V-E_T)\delta\tau]$. In practice, we sample the more accurate propagator $\exp[-(V-E_T)\delta\tau/2]\exp[-T\delta\tau]\exp[-(V-V_T)\delta\tau/2]$, that implies two sets of rotations in $\delta\tau/2$, the first depending on R and the second on the diffused R' , for a total of 30 auxiliary fields. Compared to GFMC, where the coordinates are sampled and the spin and isospin states are explicitly included and summed, in AFDMC spin and isospin are also sampled via Hubbard-Stratonovich rotations. This largely reduce the computational cost of the imaginary time propagation of a many-body wave function, allowing one to calculate more efficiently nuclei up ^{12}C , and to go beyond $A = 12$.

B. Propagation of spin-orbit operators

The spin-orbit operator reads

$$v_{LS}(r_{ij}) = v_7(r_{ij}) \mathbf{L} \cdot \mathbf{S}, \quad (40)$$

where \mathbf{L} and \mathbf{S} are defined in Eqs. (5) and (6), respectively. As shown in Ref. [35], one way to evaluate the propagator for spin-orbit operators is to consider the expansion at first order in $\delta\tau$

$$e^{-v_7(r_{ij}) \mathbf{L} \cdot \mathbf{S} \delta\tau} \approx \mathbb{1} - v_7(r_{ij}) \mathbf{L} \cdot \mathbf{S} \delta\tau, \quad (41)$$

acting on the free propagator G_0 of Eq. (27). The resulting propagator is

$$G_{LS} \approx e^{\sum_{i \neq j} \frac{1}{8i} \frac{2m}{\hbar^2} v_7(r_{ij}) (\mathbf{r}_i - \mathbf{r}_j) \times (\Delta \mathbf{r}_i - \Delta \mathbf{r}_j) \cdot (\boldsymbol{\sigma}_i + \boldsymbol{\sigma}_j)}, \quad (42)$$

where $\Delta \mathbf{r}_i = \mathbf{r}_i - \mathbf{r}'_i$ is the difference of the particle position before and after the action of the free propagator G_0 . Note that the above propagator is only linear in the spin, i.e. it does not require any auxiliary field to be sampled. However, it can be shown that it induces spurious counter terms [9]. These can be removed by using the modified propagator:

$$G_{LS} \approx e^{\sum_{i \neq j} \frac{1}{4i} \frac{m}{\hbar^2} v_7(r_{ij}) [\mathbf{r}_{ij} \times \Delta \mathbf{r}_{ij}] \cdot \boldsymbol{\sigma}_i} \times e^{-\frac{1}{2} \left[\sum_{i \neq j} \frac{1}{4i} \frac{m}{\hbar^2} v_7(r_{ij}) [\mathbf{r}_{ij} \times \Delta \mathbf{r}_{ij}] \cdot \boldsymbol{\sigma}_i \right]^2}. \quad (43)$$

This alternative version of the spin-orbit propagator contains quadratic spin operators, and thus it requires additional Hubbard-Stratonovich fields to be sampled, but it is correct at order $\delta\tau$.

C. Propagation of three-body forces

Several terms of the three-body interaction (7) can be directly included in the AFDMC propagator. These are $V_a^{2\pi,P}$, $V^{2\pi,S}$, V_D , and V_E of Eqs. (9) and (11)–(13), that correspond to terms involving only quadratic spin and isospin operators. These have the same operator structure of the spin/isospin-dependent part of the two-body potential (34). The dependence on the third particle k enters only in the radial functions $\mathcal{X}_{i\alpha j\beta}$, $\mathcal{Z}_{ij\alpha}$, and $\delta_{R_0}(r)$, that can be absorbed in the definition of the matrices $A_{ij}^{(\tau)}$ and $A_{i\alpha j\beta}^{(\sigma\tau)}$.

The structure of $V_c^{2\pi,P}$ contains instead cubic spin and isospin operators, and the Hubbard-Stratonovich transformation of Eq. (33) cannot be applied. It follows that these terms cannot be exactly included in the standard AFDMC propagation. It may be possible to invoke more complicated algorithms to sample them, but the imaginary time step will need to be higher order in $\delta\tau$. However, their expectation value can always be calculated, and it can be used to derive an approximate three-body propagator for $V_c^{2\pi,P}$.

Let's define an effective Hamiltonian H' that can be exactly included in the AFDMC propagation:

$$H' = H - V_c^{2\pi,P} + \alpha_1 V_a^{XX} + \alpha_2 V_D^{X\delta} + \alpha_3 V_E. \quad (44)$$

The three constants α_i are adjusted in order to have:

$$\begin{aligned} \langle V_c^{XX} \rangle &\approx \langle \alpha_1 V_a^{XX} \rangle, \\ \langle V_c^{X\delta} \rangle &\approx \langle \alpha_2 V_D^{X\delta} \rangle, \\ \langle V_c^{\delta\delta} \rangle &\approx \langle \alpha_3 V_E \rangle, \end{aligned} \quad (45)$$

where $\langle \dots \rangle$ indicates the average over the wave function (see Section IV E), and the identifications are suggested by the similar ranges and functional forms.

Once the ground state Ψ'_0 of H' is calculated via the AFDMC imaginary time propagation, the expectation value of the Hamiltonian H is given by

$$\begin{aligned} \langle H \rangle &\approx \langle \Psi'_0 | H' | \Psi'_0 \rangle + \langle \Psi'_0 | H - H' | \Psi'_0 \rangle \\ &\approx \langle H' \rangle + \langle V_c^{2\pi,P} - \alpha_1 V_a^{XX} - \alpha_2 V_D^{X\delta} - \alpha_3 V_E \rangle \\ &\approx \langle H' \rangle + \langle V_{\text{pert}} \rangle, \end{aligned} \quad (46)$$

where the last term is evaluated perturbatively, meaning that its expectation value is calculated, even though not all the operators are included in the propagator ($V_c^{2\pi,P}$). By opportunely adjusting the constants α_i as in Eq. (45) we ensure that the correction $\langle V_{\text{pert}} \rangle$ is small compared

to $\langle H' \rangle$. A similar approach is used in GFMC to calculate the small non-local terms that are present in the v_{18} interaction. In that case the difference $v_8^* - v_{18}$ is calculated as a perturbation [36].

D. Importance sampling

DMC algorithms, such as GFMC and AFDMC, are much more efficient when the *importance sampling* techniques is also implemented. In fact, sampling spacial and spin/isospin configurations according to $G(R', R, S'(X), S, \delta\tau)$ might not always be efficient. For instance, consider the case of a strongly repulsive interac-

tion at short distances. In such a situation, sampling the spacial coordinates according to the kinetic energy only is not an optimal choice because no information about the interaction is included in sampling the paths, but only through the weight associated to the configurations. As a result, an inefficiently sampled path might have a very small weight, making its contribution very small along the imaginary time.

Suppose to know a positive definite wave function Ψ_G close to that of the true ground state of the Hamiltonian H . Ψ_G can be used to guide the imaginary time evolution by defining a better propagator compared to that of Eq. (23), to be used to sample coordinates and spin/isospin configurations:

$$\begin{aligned} \langle \Psi_G | R' S' \rangle \langle R' S' | \Psi(\delta\tau) \rangle &= \int dR G(R', R, S'(X), S, \delta\tau) \langle \Psi_G | R' S'(X) \rangle \langle RS | \Psi_T(0) \rangle \\ &= \int dR G(R', R, S'(X), S, \delta\tau) \frac{\langle \Psi_G | R' S'(X) \rangle}{\langle \Psi_G | RS \rangle} \langle \Psi_G | RS \rangle \langle RS | \Psi_T(0) \rangle. \end{aligned} \quad (47)$$

Note that if Ψ_G is positive definite, the above propagation does not change the variance of the computed observables.

In usual DMC calculations the modified propagator is sampled by shifting the Gaussian in the free propagator, and then including the local energy in the weight of the configuration (see for example [37]). A similar approach has also been used in AFDMC in the past. However, in the latest implementation of AFDMC, a much more efficient way to implement the importance sampling propagator is used.

The goal is to sample the modified propagator:

$$G(R', R, S'(X), S, \delta\tau) \frac{\langle \Psi_G | R' S'(X) \rangle}{\langle \Psi_G | RS \rangle}. \quad (48)$$

We first sample a set of coordinate displacements ΔR according to Eq. 39 and a set of auxiliary fields X from Gaussian distributions. Since the propagator G implies the Gaussian sampling for the kinetic energy and for the auxiliary fields, sampling ΔR and X has the same probability of sampling $-\Delta R$ and $-X$. Driven by this observation, we calculate the ratios:

$$\begin{aligned} w_1 &= \frac{\langle \Psi_G | R + \Delta R, S'(X) \rangle}{\langle \Psi_G | RS \rangle} e^{-[V_{SI}(R+\Delta R) - E_T]\delta\tau}, \\ w_2 &= \frac{\langle \Psi_G | R - \Delta R, S'(X) \rangle}{\langle \Psi_G | RS \rangle} e^{-[V_{SI}(R-\Delta R) - E_T]\delta\tau}, \\ w_3 &= \frac{\langle \Psi_G | R + \Delta R, S'(-X) \rangle}{\langle \Psi_G | RS \rangle} e^{-[V_{SI}(R+\Delta R) - E_T]\delta\tau}, \\ w_4 &= \frac{\langle \Psi_G | R - \Delta R, S'(-X) \rangle}{\langle \Psi_G | RS \rangle} e^{-[V_{SI}(R-\Delta R) - E_T]\delta\tau}, \end{aligned} \quad (49)$$

where V_{SI} is the spin/isospin independent part of the interaction. We then sample one of the above choices according to the ratios w_i . Finally, the total weight of the new configuration is given by

$$W = \frac{1}{4} \sum_i w_i, \quad (50)$$

and W is used for branching as in standard DMC [1].

E. Observables

The expectation value of an observable \mathcal{O} is calculated by using the sampled configurations $R_i S_i$ as:

$$\langle \mathcal{O}(\tau) \rangle = \frac{\sum_i \frac{\langle R_i S_i | \mathcal{O} | \Psi_T \rangle}{W} \frac{W}{\langle R_i S_i | \Psi_T \rangle}}{\sum_i \frac{W}{\langle R_i S_i | \Psi_T \rangle}}. \quad (51)$$

The above expression is valid only for observables that commute with themselves, like the Hamiltonian. For other observables, such as radii and densities, expectation values are often calculated from *mixed* estimates

$$\langle \mathcal{O}(\tau) \rangle \approx 2 \frac{\langle \Psi_T | \mathcal{O} | \Psi(\tau) \rangle}{\langle \Psi_T | \Psi(\tau) \rangle} - \frac{\langle \Psi_T | \mathcal{O} | \Psi_T \rangle}{\langle \Psi_T | \Psi_T \rangle}, \quad (52)$$

where the first term corresponds to the DMC expectation value, and the second term is the VMC one. Equation (52) is valid for diagonal matrix elements, but it can be generalized to the case of off-diagonal matrix elements,

e.g. in transition matrix elements between different initial and final states (see Ref. [38]).

Note that the extrapolation above is small for accurate wave functions. This is the case, for instance, of closed-shell nuclei and single operators. For open-shell system, particularly for halo nuclei, the information encoded in the trial wave function may not be as accurate as that for simpler systems. This can result in a non negligible extrapolation of the mixed expectation value. An example of this behavior is provided by the nucleon radius, the VMC expectation value of which is typically larger than the DMC one for open-shell systems. One way to reduce the extrapolation of the radius mixed estimate is to use a penalty function during the optimization of the variational parameters in the trial wave function. This penalty function sets a constraint on the VMC radius so as to adjust its expectation value to the DMC estimate, reducing thus the extrapolation.

F. Constrained and unconstrained evolution

The fact that the weight W is always real and positive and that Ψ_T is complex, makes the denominator of Eq. (51) average quickly to zero. This is the well known sign problem in DMC. One way to avoid the sign problem is to use a constraint during the imaginary time evolution. In practice, a configuration is given zero weight (thus it is dropped during branching) if its real part changes sign.

In our implementation of AFDMC, we follow Ref. [39]. In sampling the propagator we calculate the weights w_i of Eq. (49) as

$$\frac{\langle \Psi_G | (R', S'(X)) \rangle}{\langle \Psi_G | RS \rangle} \rightarrow \text{Re} \left\{ \frac{\langle \Psi_T | (R', S'(X)) \rangle}{\langle \Psi_T | RS \rangle} \right\} \quad (53)$$

and we then apply the constraint by associating zero

weight to a move that results in a negative ratio. This is analogue to the *constrained-path* approximation [40], but for complex wave functions and propagators.

This constrained evolution does not suffer of sign problem, but it makes the final result dependent to the choice of Ψ_T . Moreover, it implies that the calculated energy is not necessarily an upperbound to the true ground state energy, as instead is the case of *fixed-node* approximation in real space [37, 41].

The results given by the constrained evolution can be improved by releasing the constraint and following the unconstrained evolution. After a set of configurations is generated using the constraint, the guiding function is taken as

$$\langle \Psi_G | RS \rangle = \text{Re} \{ \langle \Psi_G | RS \rangle \} + \alpha \text{Im} \{ \langle \Psi_G | RS \rangle \} \quad (54)$$

where α is a small arbitrary constant. This ensures that the ratio in the weights w_i of Eq. (49) is always positive and real. The propagation continues then according to the modified $\langle \Psi_G | RS \rangle$, and observables are calculated as before accordingly to Eq. (51). In several cases the expectation value $\langle O \rangle$ reaches a stable value independently to the imaginary time before the signal-to-noise ratio goes to zero, and the result is exact within the statistical uncertainty. This is the case for light systems, $A \leq 4$. For larger nuclei the variance grows much faster as a function of the imaginary time, so that the unconstrained evolution cannot always be followed until $\langle O \rangle$ reaches a plateau. In these cases, the final result is extrapolated using an exponential fit of the form $f(\tau) = a + b \cdot \exp(-c \cdot \tau)$ to the unconstrained Monte Carlo results. Examples of unconstrained evolution are provided in Section VIA.

V. TRIAL WAVE FUNCTION

The AFDMC trial wave function we use takes the form:

$$\langle RS | \Psi \rangle = \langle RS | \prod_{i < j} f_{ij}^1 \prod_{i < j < k} f_{ijk}^{3c} \left[1 + \sum_{i < j} \sum_{p=2}^6 f_{ij}^p \mathcal{O}_{ij}^p f_{ij}^{3p} + \sum_{i < j < k} U_{ijk} \right] | \Phi \rangle_{J^\pi, T}, \quad (55)$$

where $|RS\rangle$ represents the sampled $3A$ spacial coordinates and the $4A$ spin/isospin amplitudes for each nucleon, and the pair correlation functions $f_{ij}^{p=1,6} \equiv f^{p=1,6}(r_{ij})$ are obtained as the solution of Schrödinger-like equations in the relative distance between two particles, as explained in Ref. [1]. The two spin/isospin-

independent functions f_{ijk}^{3c} and f_{ij}^{3p} are defined as

$$\begin{aligned} f_{ijk}^{3c} &= 1 + q_1^c \mathbf{r}_{ij} \cdot \mathbf{r}_{ik} \mathbf{r}_{ji} \cdot \mathbf{r}_{jk} \mathbf{r}_{ki} \cdot \mathbf{r}_{kj} e^{-q_2^c(r_{ij}+r_{ik}+r_{jk})}, \\ f_{ij}^{3p} &= \prod_k \left[1 - q_1^p (1 - \mathbf{r}_{ik} \cdot \mathbf{r}_{jk}) e^{-q_2^p(r_{ij}+r_{ik}+r_{jk})} \right], \end{aligned} \quad (56)$$

and they are introduced to reduce the strength of the spin/isospin-dependent pair correlation functions when other particles are nearby [36]. Finally, three-body

spin/isospin-dependent correlations are also included as

$$U_{ijk} = \sum_n \epsilon_n V_{ijk}^n(\alpha_n r_{ij}, \alpha_n r_{ik}, \alpha_n r_{jk}), \quad (57)$$

where the terms V_{ijk}^n are the same of the three-body interactions of Eq. (7), ϵ_n are potential quenching factors, and α_n coordinate scaling factors. In the correlations above, we include the four terms $V_a^{2\pi,P}$, $V^{2\pi,S}$, V_D , and V_E . $V_c^{2\pi,P}$ can also be implemented in the trial wave function, but since its structure involves three-body spin/isospin operators, its inclusion results in a severely larger computational cost.

The term $|\Phi\rangle$ is taken as a shell-model-like wave function. It consists of a sum of Slater determinants constructed using single particle orbitals:

$$\langle RS|\Phi\rangle_{J^\pi,T} = \sum_n c_n \left[\sum_{JM} \mathcal{D}\{\phi_\alpha(\mathbf{r}_i, s_i)\}_{J,M} \right]_{J^\pi,T}, \quad (58)$$

where \mathbf{r}_i are the spacial coordinates of nucleons, and s_i represents their spinor. J is the total angular momentum, M its projection, T the total isospin, and π the parity. The determinants \mathcal{D} are coupled with Clebsch-Gordan coefficients \mathcal{C}_{JM} in order to reproduce the experimental total angular momentum, total isospin, and parity (J^π, T). The c_n are variational parameters multiplying different components having the same quantum numbers. Each single particle orbital ϕ_α consists in a radial function multiplied by the spin and isospin trial states:

$$\phi_\alpha(\mathbf{r}_i, s_i) = \Phi_{nj}(r_i) [Y_{l,m_l}(\hat{\mathbf{r}}_i) \chi_\gamma(s_i)]_{j,m_j}, \quad (59)$$

where the spherical harmonics $Y_{l,m_l}(\hat{\mathbf{r}}_i)$ are coupled to the spin state $\chi_\gamma(s_i)$ in order to have single particle orbitals in the j basis. The radial parts $\Phi(r)$ are obtained from the bound-state solutions of the Woods-Saxon wine-bottle potential:

$$v(r) = V_s \left[\frac{1}{1 + e^{(r-r_s)/a_s}} + \alpha_s e^{-(r/\rho_s)^2} \right], \quad (60)$$

where the five parameters V_s , r_s , a_s , α_s , and ρ_s can be different for orbitals belonging to different states, like $1S_{1/2}$, $1P_{3/2}$, $1P_{1/2}$, ..., and they are optimized in order to minimize the variational energy. Finally, the spin/isospin trial states are represented in the $|p \uparrow\rangle$, $|p \downarrow\rangle$, $|n \uparrow\rangle$, $|n \downarrow\rangle$ basis ($|\chi_{\gamma=1,4}\rangle$). The spinor are specified as:

$$|s_i\rangle \equiv \begin{pmatrix} a_i \\ b_i \\ c_i \\ d_i \end{pmatrix} = a_i |p \uparrow\rangle + b_i |p \downarrow\rangle + c_i |n \uparrow\rangle + d_i |n \downarrow\rangle, \quad (61)$$

and the trial spin/isospin states are taken to be:

$$\begin{aligned} \chi_1(s_i) &= \langle s_i | \chi_1 \rangle = \langle s_i | (1, 0, 0, 0) \rangle = a_i, \\ \chi_2(s_i) &= \langle s_i | \chi_2 \rangle = \langle s_i | (0, 1, 0, 0) \rangle = b_i, \\ \chi_3(s_i) &= \langle s_i | \chi_3 \rangle = \langle s_i | (0, 0, 1, 0) \rangle = c_i, \\ \chi_4(s_i) &= \langle s_i | \chi_4 \rangle = \langle s_i | (0, 0, 0, 1) \rangle = d_i. \end{aligned} \quad (62)$$

Let's consider a system with K states. According to the definitions above, a single Slater determinant $\mathcal{D} \equiv \mathcal{D}\{\phi_\alpha(\mathbf{r}_i, s_i)\}_{J,M}$ is constructed as:

$$\mathcal{D} = \begin{vmatrix} a_1 \phi_1(\mathbf{r}_1) & a_2 \phi_1(\mathbf{r}_2) & \dots & a_A \phi_1(\mathbf{r}_A) \\ a_1 \phi_2(\mathbf{r}_1) & a_2 \phi_2(\mathbf{r}_2) & \dots & a_A \phi_2(\mathbf{r}_A) \\ \dots & \dots & \dots & \dots \\ b_1 \phi_1(\mathbf{r}_1) & b_2 \phi_1(\mathbf{r}_2) & \dots & b_A \phi_1(\mathbf{r}_A) \\ b_1 \phi_2(\mathbf{r}_1) & b_2 \phi_2(\mathbf{r}_2) & \dots & b_A \phi_2(\mathbf{r}_A) \\ \dots & \dots & \dots & \dots \\ d_1 \phi_1(\mathbf{r}_1) & d_2 \phi_1(\mathbf{r}_2) & \dots & d_A \phi_1(\mathbf{r}_A) \\ \dots & \dots & \dots & \dots \\ d_1 \phi_K(\mathbf{r}_1) & d_2 \phi_K(\mathbf{r}_2) & \dots & d_A \phi_K(\mathbf{r}_A) \end{vmatrix}. \quad (63)$$

For ^{16}O ($0^+, 0$), for instance, the number of states is four: one $1S_{1/2}$, two $1P_{3/2}$, and one $1P_{1/2}$. Each of them can accommodate two spins and two isospin states, and the full $\langle RS|\Phi\rangle_{0^+,0}$ wave function can be written as a single Slater determinant. For open shell systems instead, many Slater determinants need to be included in order to have a good trial wave function with the proper (J^π, T). For $A = 6$ systems, for example, including single particle orbitals up to the sd shell there are ten possible states: one $1S_{1/2}$, two $1P_{3/2}$, one $1P_{1/2}$, three $1D_{5/2}$, two $1D_{3/2}$, and one $2S_{1/2}$. These can be combined in 9 different Slater determinants in order to have the ^6He ($0^+, 1$) wave function, or in 32 Slater determinants to make ^6Li ($1^+, 0$). Finally, for ^{12}C ($0^+, 0$), by considering only $K = 4$ as for ^{16}O ($0^+, 0$), the number of Slater determinants needed to build a ($0^+, 0$) wave function is already 119, making it computationally challenging to include sd shell orbitals for $A = 12$.

The trial wave function of Eq. (55) contains a sum over pair correlation functions, meaning that only a pair of nucleons ij is correlated at a time (linear correlations). This is different compared to the GFMC wave function [1], where all pairs are correlated at the same time. This construction, however, forbids the application of the Hubbard-Stratonovich transformation in AFDMC, justifying the choice of Eq. (55). An improved AFDMC two-body wave function could include linear and quadratic pair correlations:

$$\langle RS|\Psi\rangle_{2b} = \langle RS|\prod_{i<j} f_{ij}^1 \left[1 + \sum_{i<j} \sum_{p=2}^6 f_{ij}^p \mathcal{O}_{ij}^p + \sum_{i<j} \sum_{p=2}^6 f_{ij}^p \mathcal{O}_{ij}^p \sum_{\substack{k<l \\ ij \neq kl}} \sum_{q=2}^6 f_{kl}^q \mathcal{O}_{kl}^q \right] |\Phi\rangle_{J^\pi, T}, \quad (64)$$

where the sum over kl includes all nucleon pairs except when $k = i$ and $l = j$. The $f_{ij}^{p,q}$ functions are solved for as before, and the operators $\mathcal{O}_{ij}^{p,q}$ are the same of Eq. (55). Although the two-body wave function of Eq. (64) contains all quadratic correlations, most of the relevant physics is captured with a subset of these correlations, corresponding to the action of the $\mathcal{O}_{ij}^{p,q}$ operators on four distinct particles—*independent pair correlations*. Since these correlations never act on the same particle, all the $\mathcal{O}_{ij}^{p,q}$ operators commute, removing the need for an explicit symmetrization of the wave function. Such a wave function could, in principle, improve the energy expectation value for large systems, but the computational cost of its evaluation is severely increased. In fact, the cost of computing expectation values of two-body operators on a two-body wave function of the form (64) is proportional to A^4 for linear correlations, and to A^6 for quadratic correlations. For this reason in the present work we consider only linear two-body correlations in the wave function, and we present a test study of quadratic correlations in Section VIB.

VI. RESULTS

A. Test of constrained and unconstrained evolution

As introduced in Section IVF, the energy (and other observables) calculated with AFDMC during the constrained evolution is dependent of the choice of Ψ_T . This is shown in Table I where the energy of ${}^4\text{He}$ is calculated for the Argonne v6' (AV6') potential [32] employing different trial wave functions. *Full w.f.* refers to the wave function of Eq. (55) where all the two-body correlations are included. *Simple w.f.* is instead a simplified wave function where only the central and $p = 2, 5$ operator correlations are used, the strength of the latter ($\mathcal{O}_{ij}^5 = S_{ij} \boldsymbol{\tau}_i \cdot \boldsymbol{\tau}_j$) being artificially reduced by a factor 3 after the optimization process. At the variational level it is evident how the simplified wave function is not the optimal choice for Ψ_T , being the energy expectation value much higher than for the fully optimized wave function. For both choices of Ψ_T , the constrained evolution reduces the binding energy, moving towards the GFMC reference value for the same potential (see Tab. II), but the results are still inconsistent. It is only the unconstrained evolution that brings the results for both wave functions in agreement within statistical errors. This is also shown in Fig. 1, where the AFDMC energy is plotted as func-

tion of the imaginary time step for the unconstrained evolution.

Table I. ${}^4\text{He}$ ground state energies for the AV6' potential and different trial wave functions (see text for details). C(U) refers to the constrained(unconstrained) evolution. Errors are statistical. Results are in MeV.

Energy	Simple w.f.	Full w.f.
E_{VMC}	-9.49(5)	-23.35(1)
$E_{\text{AFDMC}}^{\text{C}}$	-25.28(3)	-26.45(1)
$E_{\text{AFDMC}}^{\text{U}}$	-26.34(12)	-26.31(4)

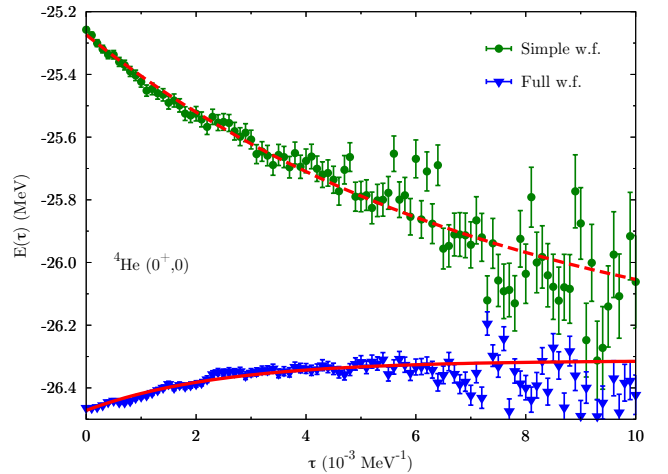


Figure 1. Energy of ${}^4\text{He}$ as a function of the imaginary time after releasing the constraint for the AV6' potential. The two data sets refer to the two different wave functions of Table I. Red lines are exponential fits to the Monte Carlo results leading to the energy values $E_{\text{AFDMC}}^{\text{U}}$ of Table I.

We report in Table II the constrained and unconstrained energies for $A = 3, 4, 6$ employing the AV6' potential, in comparison with the GFMC results for the same interaction [32]. It is interesting to note that constrained energies do not always satisfy the variational principle, as anticipated in Section IVF. This is seen, for example, in ${}^3\text{H}$ and ${}^4\text{He}$, for which the constrained energy is below the GFMC prediction, considered to be the exact solution for the given potential. However, once the unconstrained evolution is performed, AFDMC and GFMC results agree within 1% or less.

In Figs. 2 and 3 we show two examples of uncon-

Table II. Ground state energies for $A = 3, 4, 6$ employing the AV6' potential. Errors are statistical. Results are in MeV.

${}^Z\text{A} (J^\pi, T)$	$E_{\text{AFDMC}}^{\text{C}}$	$E_{\text{AFDMC}}^{\text{U}}$	E_{GFMC}
${}^3\text{H} (\frac{1}{2}^+, \frac{1}{2})$	-8.08(1)	-7.95(2)	-7.95(2)
${}^4\text{He} (0^+, 0)$	-26.45(1)	-26.31(4)	-26.15(2)
${}^6\text{Li} (1^+, 0)$	-28.09(4)	-28.26(10)	-28.37(4)

strained calculation for larger systems, ${}^6\text{He}$ and ${}^{16}\text{O}$ respectively, employing realistic two- plus three-body interactions. We use the local chiral potential at N^2LO with cutoff $R_0 = 1.2\text{ fm}$ for ${}^6\text{He}$ and $R_0 = 1.0\text{ fm}$ for ${}^{16}\text{O}$. The employed wave functions include all two- and three-body correlations, and for ${}^6\text{He}$ we include single particle orbitals up to the sd shell. In general, the larger the system, the shorter the imaginary time evolution that can be followed before the variance becomes too large. This is particularly evident in ${}^{16}\text{O}$ for which the unconstrained evolution can be satisfactorily performed up to $2.5 \times 10^{-4}\text{ MeV}^{-1}$, compared to the $4 \times 10^{-4}\text{ MeV}^{-1}$ for ${}^6\text{He}$ of Fig. 2, and to the $5 \times 10^{-3}\text{ MeV}^{-1}$ (10^{-2} MeV^{-1}) for ${}^4\text{He}$ with the same interaction (with AV6'), Fig. 1. For example, at $\tau = 2 \times 10^{-4}\text{ MeV}^{-1}$ the statistical error per nucleon is 0.01 MeV for ${}^4\text{He}$ and ${}^6\text{Li}$, and 0.19 MeV for ${}^{16}\text{O}$. This is a direct consequence of the quality of the employed wave function. For small nuclei, the wave function of Eq. (55) provides a good description of the system, and the energy expectation value of the constrained evolution is already close to the expected result. In ${}^6\text{He}$ the difference between constrained and unconstrained energy is of the order of 1 MeV, roughly 3% of the final result. In ${}^{16}\text{O}$ instead, the constrained energy is higher, and the unconstrained evolution lowers its value of about 25 MeV, $\approx 22\%$ of the total energy. This could be improved by employing more sophisticated wave functions including higher order correlations, such as that of Eq. (64), and/or using more refined techniques to perform the unconstrained evolution. Studies along these directions are underway.

B. Test of quadratic two-body correlations

The results presented in the previous section are obtained using a trial wave function of the form (55), i.e. by retaining only two-body linear correlations in $\langle RS|\Psi\rangle$. We present in Table III a test study on the effect of including quadratic correlations in the wave function to the energy expectation value. The energy expectation values for the constrained evolution have been calculated for ${}^4\text{He}$, ${}^{16}\text{O}$, and symmetric nuclear matter (SNM) with 28 particles in a box with periodic boundary conditions at saturation density $\rho_0 = 0.16\text{ fm}^{-3}$. We use the AV6' potential with no Coulomb interaction for all the systems. Results are shown for the linear, independent pair, and full quadratic two-body correlations.

Though there is little difference in ${}^4\text{He}$, the constrained

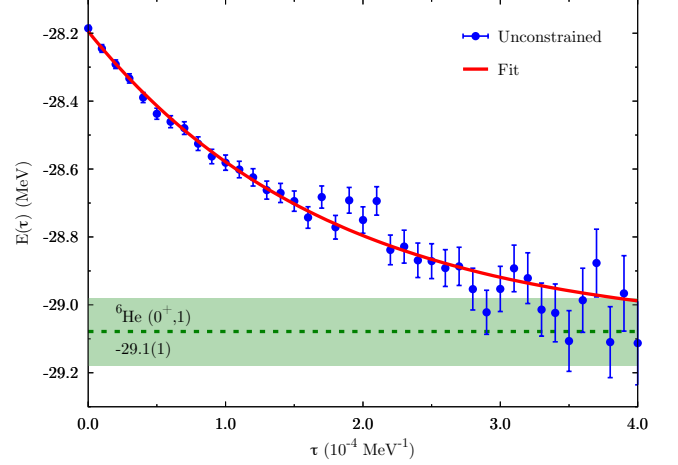


Figure 2. ${}^6\text{He}$ unconstrained evolution for the local chiral potential at N^2LO ($E\tau$) with cutoff $R_0 = 1.2\text{ fm}$. Data points refer to the expectation value of H' , Eq. (44).

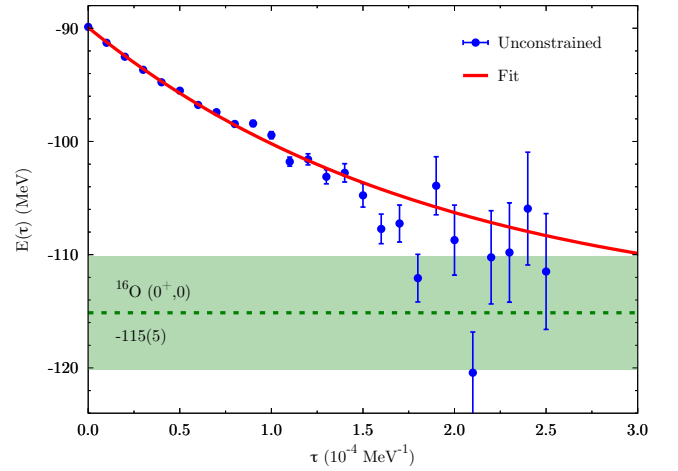


Figure 3. ${}^{16}\text{O}$ unconstrained evolution for the local chiral potential at N^2LO ($E\tau$) with cutoff $R_0 = 1.0\text{ fm}$. Data points refer to the expectation value of H' , Eq. (44).

energies for both ${}^{16}\text{O}$ and SNM are lower when employing quadratic correlations, particularly for SNM. In ${}^{16}\text{O}$ the energy gain for the constrained evolution is only $\approx 0.3(1)\text{ MeV/A}$, while in SNM this value increases up to $\approx 0.8(1)\text{ MeV/A}$. No difference is found, within statistical uncertainties, between independent pair and full quadratic correlations results, except for the higher computational cost of the latter. To be noted that the variational parameters in the trial wave function (64) were re-optimized for ${}^4\text{He}$. In the case of ${}^{16}\text{O}$ and SNM instead, due to the cost of optimizing such parameters using the full wave function of Eq. (64), we used the same parameters obtained for the linear wave function (55).

Table III. Energy per nucleon (in MeV) for ${}^4\text{He}$, ${}^{16}\text{O}$, and SNM at ρ_0 . The employed potential is AV6'. No Coulomb interaction is considered here. Results are shown for the linear, independent pair, and full quadratic two-body correlations. Errors are statistical.

System	Linear	Ind-Pair	Quadratic
${}^4\text{He}$	-6.79(1)	-6.81(1)	-6.78(1)
${}^{16}\text{O}$	-7.23(6)	-7.59(9)	-7.50(9)
SNM	-13.92(6)	-14.80(7)	-14.70(11)

C. Fit of the three-body interaction

Original reference [22]

Table IV. Cutoff.

V_{ijk}	R_0 (fm)	c_D	c_E
$E\tau$	1.0	0.0	-0.63
	1.2	3.5	0.09
$E1$	1.0	0.5	0.62
	1.2	-0.75	0.025

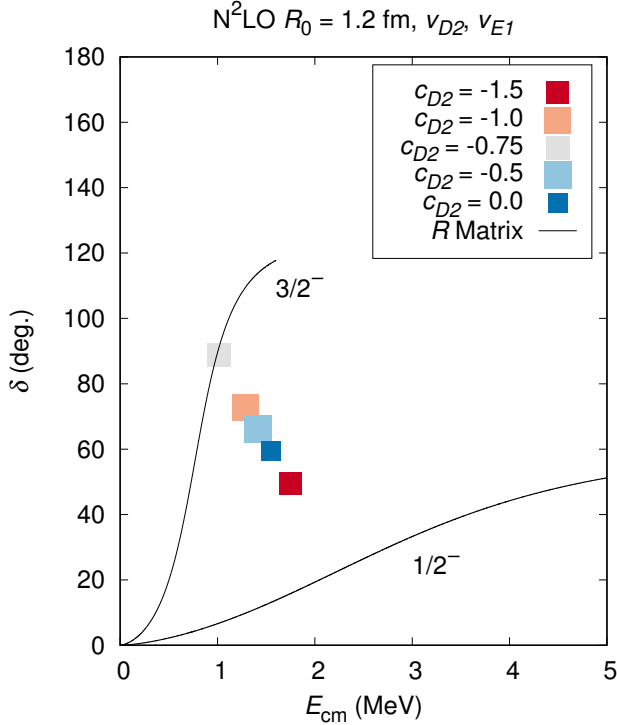


Figure 4. Test image.

D. Test of the three-body calculation

The energies reported in Figs. 2 and 3 correspond to the expectation values of the effective Hamiltonian H' , Eq. (44). These need to be adjusted with the perturbative correction of Eq. (46)—also extracted from the unconstrained evolution—in order to obtain the final results reported in Tables VIII and IX. Once the optimal set of parameters α_i is found, these corrections are small, almost consistent with zero within Monte Carlo statistical uncertainties, as shown in Table V.

Table V. Energy expectation values of Eq. (46) for $A \geq 6$. Errors are statistical. Results are in MeV.

${}^Z A (J^\pi, T)$	N^2LO	R_0 (fm)	$\langle H' \rangle$	$\langle V_{\text{pert}} \rangle$	$\langle H \rangle$
${}^6\text{He} (0^+, 1)$	$E\tau$	1.0	-28.3(4)	0.1(2)	-28.4(4)
		1.2	-29.1(1)	0.2(1)	-29.3(1)
	$E1$	1.0	-28.5(5)	-0.3(2)	-28.2(5)
		1.2	-27.0(1)	—	—
${}^6\text{Li} (1^+, 0)$	$E\tau$	1.0	-31.2(4)	0.3(3)	-31.5(5)
		1.2	-31.9(3)	0.4(1)	-32.3(3)
	$E1$	1.0	-30.9(4)	-0.2(2)	-30.7(4)
		1.2	—	—	—
${}^{12}\text{C} (0^+, 0)$	$E\tau$	1.0	-75(2)	3(1)	-78(3)
${}^{16}\text{O} (0^+, 0)$	$E\tau$	1.0	-115(5)	2(1)	-117(5)
		1.2	-265(25)	-2(6)	-263(26)
	$E1$	1.0	-106(6)	1(1)	-107(6)
		1.2	-114(8)	-2(2)	-112(8)

The final result $\langle H \rangle$ is, however, nearly independent to variations of the α_i parameters, even for larger systems. This is shown in Table VI where the α_i are arbitrarily changed in ${}^{16}\text{O}$ within 5–10% with respect to the optimal values, given in the first row for each cutoff. This results in $\lesssim 4\%$ variations of the total energy, compatible with the overall Monte Carlo statistical uncertainties. To be noted that, in order to save computing time, this test has been done using the constrained evolution. However, the optimal constrained expectation values $\langle V_{\text{pert}} \rangle$ are consistent with the unconstrained ones of Table V.

Unless differently specified, in the following all ground state energies will correspond to the final expectation value $\langle H \rangle$, extracted from the unconstrained Monte Carlo results for $\langle H' \rangle$ with an exponential fit, and adjusted with the perturbative correction of Eq. (46) when three-body forces are employed.

E. Ground state energies and charge radii

We consider local chiral Hamiltonians at leading-order (LO), next-to-leading-order (NLO), and N^2LO , the latter including both two- and three-body forces. At each order we can assign theoretical uncertainties to observables coming from the truncation of the chiral expansion [42].

Table VI. Contributions to the energy expectation value of Eq. (46) in ^{16}O . The parametrization $E\tau$ of the three-body force is used for different cutoffs. $\langle V_{\text{pert}} \rangle$ is the proper mixed estimator. For each cutoff, the first line represents the optimal choice for α_i . Energies (in MeV) are the result of the constrained evolution. Errors are statistical.

R_0 (fm)	$(\alpha_1, \alpha_2, \alpha_3)$	$\langle H' \rangle$	$\langle V_{\text{pert}} \rangle$	$\langle H \rangle$
1.0	(2.05, -3.80, -0.95)	-90.0(3)	1.8(5)	-91.8(6)
	(2.50, -3.30, -1.20)	-125.1(6)	-33.9(8)	-92.2(1.0)
	(1.95, -4.00, -0.90)	-83.3(2)	5.9(9)	-89.2(1.0)
	(1.80, -4.20, -0.85)	-75.6(3)	13.9(1.4)	-89.4(1.5)
1.2	(1.80, 0.45, 8.00)	-171(2)	-2(1)	-169(2)
	(1.90, 0.50, 8.50)	-197(3)	-25(2)	-172(3)
	(1.70, 0.40, 7.50)	-147(1)	15(1)	-162(1)

For an observable X at N^2LO , the theoretical uncertainty is obtained as

$$\Delta X^{\text{N}^2\text{LO}} = \max(Q^4 \times |X^{\text{LO}}|, Q^2 \times |X^{\text{NLO}} - X^{\text{LO}}|, Q \times |X^{\text{N}^2\text{LO}} - X^{\text{NLO}}|), \quad (65)$$

where we take $Q = m_\pi/\Lambda_b$ with $m_\pi \approx 140$ MeV and $\Lambda_b = 600$ MeV, as done in [22, 31].

The expectation value of the charge radius is derived from the point-proton radius using the relation:

$$\langle r_{\text{ch}}^2 \rangle = \langle r_{\text{pt}}^2 \rangle + \langle R_p^2 \rangle + \frac{A-Z}{Z} \langle R_n^2 \rangle + \frac{3\hbar^2}{4M_p^2 c^2}, \quad (66)$$

where r_{pt} is the calculated point-proton radius, $\langle R_p^2 \rangle = 0.770(9) \text{ fm}^2$ [43] the proton radius, $\langle R_n^2 \rangle = -0.116(2) \text{ fm}^2$ [43] the neutron radius, and $(3\hbar^2)/(4M_p^2 c^2) \approx 0.033 \text{ fm}^2$ the Darwin-Foldy correction [44]. For ^6He a spin-orbit correction $\langle r_{\text{so}}^2 \rangle = -0.08 \text{ fm}^2$ [45] is also included. The point-nucleon radius r_{pt} is calculated as

$$\langle r_N^2 \rangle = \frac{1}{\mathcal{N}} \langle \Psi | \sum_i \mathcal{P}_{N_i} |\mathbf{r}_i - \mathbf{R}_{\text{cm}}|^2 | \Psi \rangle, \quad (67)$$

where \mathbf{R}_{cm} is the coordinate of the center of mass of the system, \mathcal{N} is the number of protons or neutron, and

$$\mathcal{P}_{N_i} = \frac{1 \pm \tau_{z_i}}{2}, \quad (68)$$

is the projector operator onto protons or neutrons. The charge radius is a mixed expectation value, and it requires the calculation of both VMC and DMC point-proton radii, accordingly to Eq. (52). Regardless the employed optimization of the variational wave function (free or constrained), the extrapolation of the mixed estimate $\langle r_{\text{ch}}^2 \rangle$ is small, and the final results are typically within statistical uncertainties.

The ground state energies and charge radii for light systems ($A = 3, 4$) employing the local chiral potential at N^2LO are shown in Table VII. Results with ($E\tau$ parametrization) and without the three-body force are shown for different choices of the cutoff R_0 . For all the $s_{1/2}$ systems we used the same parameters α_i for the propagation of the three-body force, determined in order to minimize the perturbative correction of Eq. (46). The agreement with the GFMC results of Ref. [22, 26], where the three-body interactions are fully included in the propagation, is within few percent both at the two- and three-body level, providing a good benchmark for the AFDMC propagation technique described in Section IV C.

In Figs. 5 and 6 we present the ground state energies per nucleon of nuclei with $3 \leq A \leq 16$ for cutoffs $R_0 = 1.0$ fm and $R_0 = 1.2$ fm, respectively. Results at LO, NLO, and N^2LO for both $E\tau$ and $E1$ parametrizations of the three-body force are shown. Error bars are estimated by including both the Monte Carlo uncertainties and the errors given by the truncation of the chiral expansion, the latter being the dominant ones. For the hard interaction ($R_0 = 1.0$ fm), the predicted binding energies at N^2LO are in good agreement with experimental data all the way up to $A = 16$. No differences, within error bars, are found for the two different parametrizations of the three-body force.

^{12}C in the $E\tau$ parametrization is slightly underbound. This is most likely a consequence of the employed wave function that results in a too high energy for the constrained evolution. This could be due to the complicated clustering structure of ^{12}C not included in Ψ_T , that would require a much longer unconstrained propagation to filter out the corresponding low excitations from Ψ_T . For $A = 6$ the wave function is constructed using up to sd shell single-particle orbitals. For ^{12}C instead, coupling p shell orbitals only already results in a sum of 119 Slater determinants. Including orbitals in the sd shell could in principle result in a better wave function for this open-shell system, but it will sizably increase the number of determinants to consider, making the calculation prohibitively time consuming. Another possible improvement would be to include quadratic terms in the pair correlations, as shown in Eq. (64). However, first attempts in ^{16}O lead to just a $\approx 6(2)$ MeV reduction of the total energy in a simplified scenario (see Table III), with a noticeably increase of computational cost.

For the soft interaction ($R_0 = 1.2$ fm), NLO and in particular LO results are typically more bound compared to the $R_0 = 1.0$ fm case. Both parametrizations of the three-body force bring the N^2LO energies compatible with the experimental values up to $A = 6$, and consistent with those obtained with the hard potential. (to be verified in ^6He and ^6Li).

Different is the case of ^{16}O that at LO is dramatically overbound (≈ -1 GeV), implying huge theoretical errors at NLO and N^2LO coming from the prescription of Eq. (65). Within these uncertainties, NLO and N^2LO two-body energies are compatible with the corre-

Table VII. Ground state energies and charge radii for $A = 3, 4$ employing the local chiral potential at N^2LO . The $E\tau$ parametrization is used for the three-body force. Errors are statistical. GFMC results are from Refs. [22, 27].

Nucleus ${}^Z_A(J^\pi, T)$	Cutoff R_0 (fm)	Potential	AFDMC		GFMC	
			E (MeV)	r_{ch} (fm)	E (MeV)	r_{ch} (fm)
${}^3H(\frac{1}{2}^+, \frac{1}{2})$	1.0	2b	-7.54(4)	1.75(2)	-7.55(1)	1.78(2)
		2b+3b	-8.33(7)	1.72(2)	-8.34(1)	1.72(3)
	1.2	2b	-7.76(3)	1.74(2)	-7.74(1)	1.75(2)
		2b+3b	-8.27(5)	1.73(2)	-8.35(4)	1.72(4)
${}^3He(\frac{1}{2}^+, \frac{1}{2})$	1.0	2b	-6.89(5)	2.02(2)	-6.78(1)	2.06(2)
		2b+3b	-7.55(8)	1.96(2)	-7.65(2)	1.97(2)
	1.2	2b	-7.12(3)	1.98(2)	-7.01(1)	2.01(1)
		2b+3b	-7.64(4)	1.95(5)	-7.63(4)	1.97(1)
${}^4He(0^+, 0)$	1.0	2b	-23.96(8)	1.72(2)	-23.72(1)	1.73(1)
		2b+3b	-27.64(13)	1.68(2)	-28.30(1)	1.65(2)
	1.2	2b	-25.17(5)	1.69(1)	-24.86(1)	1.69(1)
		2b+3b	-28.37(8)	1.65(1)	-28.30(1)	1.64(1)

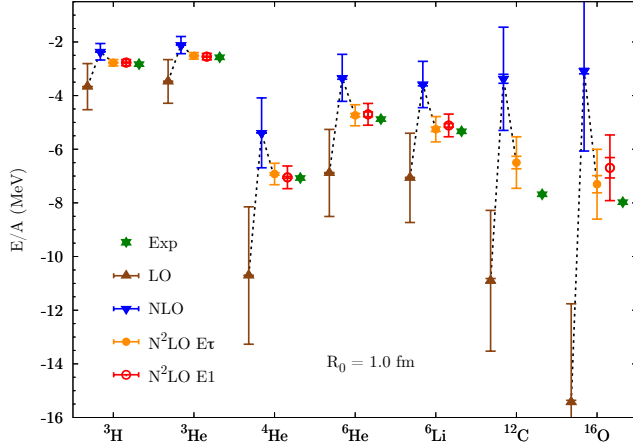


Figure 5. Ground state energies per nucleon for $3 \leq A \leq 16$ with the local chiral potential for the $R_0 = 1.0$ fm cutoff. Results at different order of the chiral expansion and for different three-body parametrizations are shown. Smaller error bars (indistinguishable from the symbols up to $A = 6$) indicate the statistical Monte Carlo uncertainty, while larger error bars are the uncertainties from the truncation of the chiral expansion. Updated from Ref. [31].

sponding results for the hard interaction (see Tables VIII and IX). However, the contribution of the three-body force at N^2LO largely depends upon the employed operator structure. The $E\tau$ parametrization for the soft potential is very attractive, adding almost 10 MeV per nucleon to the total energy, and thus predicting a severe overbinding with a ground state energy of ≈ -260 MeV. The $E1$ parametrization is instead less attractive, resulting in a 0.3 MeV per nucleon more binding with respect to the two-body case (to be verified), result compatible

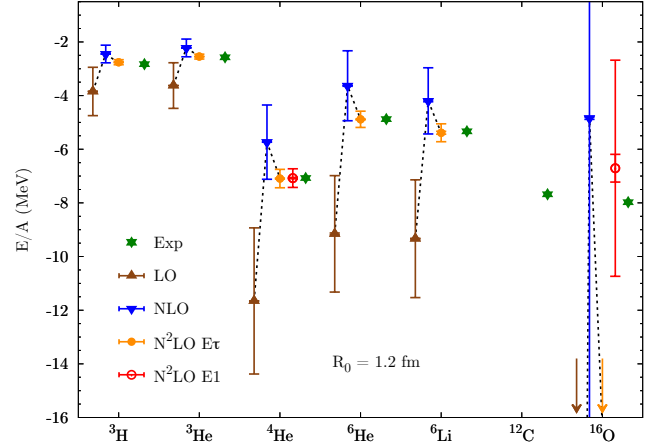


Figure 6. Same of Fig. 5 but for the $R_0 = 1.2$ fm cutoff. LO and N^2LO $E\tau$ results for ${}^{16}O$ are outside the displayed energy region.

with the energy expectation values for the hard interaction. It follows that softer local Hamiltonians manifest issues in the description of medium-mass nuclei, calling for a significant dependence on the employed operator structure and, possibly, for the necessity of inputs other than few-body observables, as already pointed out for example in Ref. [17].

Figures 7 and 8 show the charge radii at different orders of the chiral expansion and for different cutoffs and parametrizations of the three-body force. The agreement with experimental data for the hard interaction at N^2LO is remarkably good all the way up to oxygen. Exception is 6Li , for which the charge radius is somewhat underpredicted. However, a similar conclusion is found in GFMC calculations employing the AV18+IL7 potential, where

charge radii of lithium isotopes are underestimated.

For the soft interaction, the description of charge radii resembles order by order that for the hard potential up to ${}^4\text{He}$, with the N²LO results in agreement with experimental data (also shown in Table VII). The picture changes instead for $A \geq 6$, with radii progressively smaller at each order compared to the $R_0 = 1.0\text{ fm}$ case, and no longer compatible at N²LO with experimental values. The charge radius of ${}^{16}\text{O}$ turns out to be close to 2.2 fm with the soft interaction, smaller than that of ${}^6\text{Li}$ for the same potential, but consistent with the severe overbinding predicted for $A = 16$. (need the new results for $E1$ to complete this paragraph).

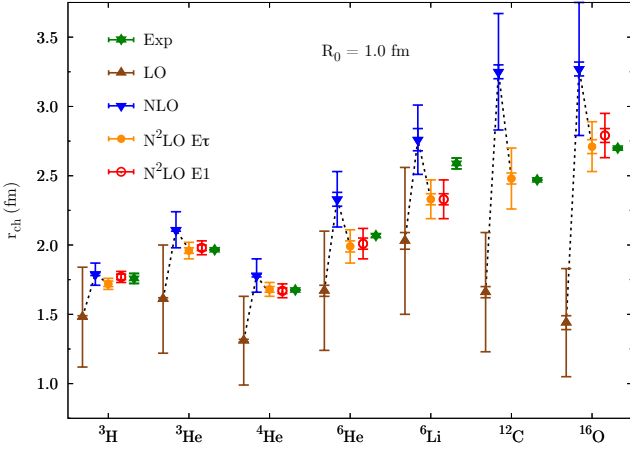


Figure 7. Charge radii for $3 \leq A \leq 16$ with the local chiral potential for the $R_0 = 1.0\text{ fm}$ cutoff. Results at different order of the chiral expansion and for different three-body parametrizations are shown. Error bars are as in Fig. 5. Updated from Ref. [31].

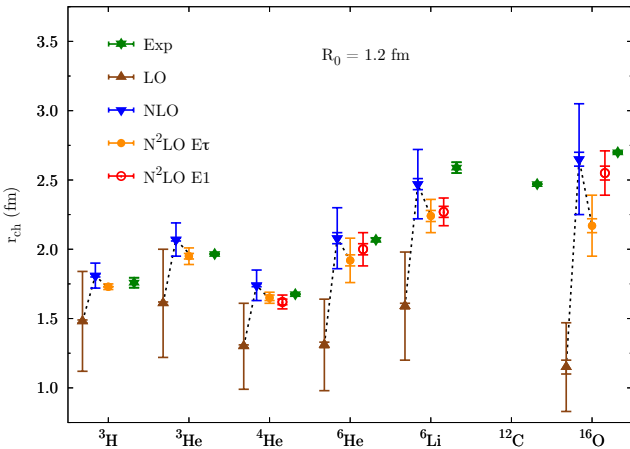


Figure 8. Same as Fig. 7 but for the $R_0 = 1.2\text{ fm}$ cutoff.

The details of LO, NLO, and N²LO calculations for

$A \geq 6$ are reported in Tables VIII and IX for $R_0 = 1.0\text{ fm}$ and $R_0 = 1.2\text{ fm}$, respectively. Results for the constrained and unconstrained evolution energies are both shown, together with the charge radius. Both Monte Carlo uncertainties and theoretical errors coming from the truncation of the chiral expansion are reported (where available). At N²LO the two-body energy is shown together with that of two different parametrizations of the three-body force ($E\tau$ and $E1$).

The full calculation of ${}^{12}\text{C}$ at N²LO required order of 10^6 CPU hours (on Intel Broadwell cores @ 2.1 GHz) for a single cutoff (1.0 fm) and three-body parametrization ($E\tau$). Due to the high computational cost, no attempts were made for the $E1$ parametrization of the three-body force or for the 1.2 fm cutoff.

As shown in Table IX, the overbinding in ${}^{16}\text{O}$ for the soft interaction appears to happen once the three-body force is included. This is more evident by looking at the detailed energy contributions for the different chiral potentials reported in Table X. (discussion to be completed with the new results for $E1$).

F. Charge form factors and Coulomb sum rules

One- and two-body point-nucleon densities are calculated as

$$\rho_N(r) = \frac{1}{4\pi r^2} \langle \Psi | \sum_i \mathcal{P}_{N_i} \delta(r - |\mathbf{r}_i - \mathbf{R}_{\text{cm}}|) | \Psi \rangle, \quad (69)$$

$$\rho_{NN}(r) = \frac{1}{4\pi r^2} \langle \Psi | \sum_{i < j} \mathcal{P}_{N_i} \mathcal{P}_{N_j} \delta(r - |\mathbf{r}_i - \mathbf{r}_j|) | \Psi \rangle, \quad (70)$$

where \mathcal{P}_{N_i} is the projector operator of Eq. (68). With the current definitions, ρ_N and ρ_{NN} integrate to the number of nucleons and the number of nucleon pairs, respectively.

Differently from the charge radius, densities are not observables themselves, but they can be related to physical quantities experimentally accessible via electron-nucleon scattering processes, such as the longitudinal elastic (charge) form factor. In fact, the charge form factor can be expressed as the ground state expectation value of the one-body charge operator [47], that, ignoring small spin-orbit contributions in the one-body current, results in the following expression:

$$F_L(q) = \frac{1}{Z} \frac{G_E^p(Q_{\text{el}}^2) \tilde{\rho}_p(q) + G_E^n(Q_{\text{el}}^2) \tilde{\rho}_n(q)}{\sqrt{1 + Q_{\text{el}}^2/(4m_N^2)}}, \quad (71)$$

where $\tilde{\rho}_N(q)$ is the Fourier transform of the one-body point-nucleon density defined in Eq. (69), and $Q_{\text{el}}^2 = \mathbf{q}^2 - \omega_{\text{el}}^2$ is the four momentum squared, with $\omega_{\text{el}} = \sqrt{q^2 + m_A^2} - m_A$ the energy transfer corresponding to the elastic peak, m_A being the mass of the target nucleus. $G_E^N(Q^2)$ are the nucleon electric form factors, for which we adopt the Kelly's parametrization [48].

The charge form factor of ${}^6\text{Li}$, ${}^{12}\text{C}$, and ${}^{16}\text{O}$ are shown in Figs. 9–11, respectively. In all the plots, the blue(red)

Table VIII. Ground state energies and charge radii for $A \geq 6$ with the local chiral potential. Results at different order of the chiral expansion and for different three-body parametrizations are shown. Energy results are shown for both the constrained (E_C) and unconstrained (E) evolutions. The first error is statistical, the second systematic. The employed cutoff is $R_0 = 1.0$ fm. Experimental charge radii are from Ref. [46].

${}^Z\text{A} (J^\pi, T)$	Potential	E_C (MeV)	E (MeV)	r_{ch} (fm)
${}^6\text{He} (0^+, 1)$	LO	-42.1(1)	-41.3(1)(9.6)	1.67(4)(39)
	NLO	-18.19(7)	-20.0(3)(5.0)	2.33(5)(15)
	N ² LO 2b	-22.24(4)	-23.1(2)(1.2)	2.11(4)(5)
	N ² LO $E\tau$	-26.58(6)	-28.4(4)(2.0)	1.99(4)(8)
	N ² LO $E1$	-26.33(8)	-28.2(5)(1.9)	2.01(4)(7)
	exp		-29.3	2.066(11)
${}^6\text{Li} (1^+, 0)$	LO	-42.8(1)	-42.4(1)(9.9)	2.03(6)(47)
	NLO	-19.2(2)	-21.5(3)(4.9)	2.76(8)(17)
	N ² LO 2b	-24.3(1)	-25.5(4)(1.1)	2.46(4)(7)
	N ² LO $E\tau$	-28.9(1)	-31.5(5)(2.3)	2.33(4)(10)
	N ² LO $E1$	-28.9(1)	-30.7(4)(2.1)	2.33(4)(10)
	exp		-32.0	2.589(39)
${}^{12}\text{C} (0^+, 0)$	LO	-131.5(2)	-131(1)(31)	1.66(4)(39)
	NLO	-31.1(2)	-41(2)(21)	3.25(5)(37)
	N ² LO 2b	-63.5(2.4)	-66(3)(6)	2.66(4)(14)
	N ² LO $E\tau$	-70.2(5)	-78(3)(9)	2.48(4)(18)
	N ² LO $E1$	—	—	—
	exp		-92.2	2.470(2)
${}^{16}\text{O} (0^+, 0)$	LO	-251.7(2)	-247(1)(58)	1.44(3)(34)
	NLO	-37.3(2)	-49(2)(46)	3.27(5)(43)
	N ² LO 2b	-72.8(2)	-87(3)(11)	2.76(5)(12)
	N ² LO $E\tau$	-91.8(6)	-117(5)(16)	2.71(5)(13)
	N ² LO $E1$	-84.5(5)	-107(6)(13)	2.79(5)(11)
	exp		-127.6	2.669(5)

curve is the AFDMC result for the N²LO $E1$ potential ($E\tau$ for ${}^{12}\text{C}$) with cutoff $R_0 = 1.0(1.2)$ fm. Monte Carlo error bars are typically of the size of the lines within the momentum range considered here. Lighter shaded areas indicate the uncertainties from the truncation of the chiral expansion, accordingly to Eq. (65). Darker shaded areas are instead the theoretical error bands only considering the last term of the prescription, i.e. taking into account the NLO and N²LO results only. AFDMC results are compared to experimental data and to available Monte Carlo calculations employing the phenomenological potentials and one-body charge operators only. No two-body operators are included in the calculation of the charge form factors in the current work. However, as shown in Refs. [49–51] for the three different systems, such operators gives a measurable contribution only for $q > 2 \text{ fm}^{-1}$, as they basically include relativistic corrections. **Comment: for the hard interaction, the corresponding cutoff in momentum space is $\approx 500 \text{ MeV}$ or $\approx 2.5 \text{ fm}^{-1}$, so there is not much room to see two-body currents effect anyway. Also, all the plots for the charge form factor seem to provide the same description as the phenomenological potentials for one-body operators up**

to $q = 3 \text{ fm}^{-3}$, already above the cutoff of the theory. Should we elaborate on this?

The charge form factor of ${}^6\text{Li}$ for the hard chiral interaction is compatible with experimental data at low momentum. The discrepancy for $q \gtrsim 2 \text{ fm}^{-1}$ is most likely due to the missing two-body currents. Similar physical picture is given for ${}^{12}\text{C}$ and ${}^{16}\text{O}$, for which the position of the first diffraction peak in the form factor is well reproduced within the band given by statistical plus theoretical uncertainties, and deviations from the experimental data occur at high momentum only. For the soft chiral interaction instead, the description of the charge form factor is less accurate, particularly for ${}^{16}\text{O}$, for which the position of the first diffraction peak is overestimated, and the slope of $F_L(q)$ for $q = 0$ is underestimated, as reflected by the smaller charge radius compared to the experimental value. The full truncation error estimate is provided for all the three nuclei (light bands). The difference between lighter and darker areas is determined by LO contributions to the theoretical error estimate, that are particularly important for the soft cutoff. Finally, it is interesting to note that for all three systems, the local chiral interaction with cutoff $R_0 = 1.0$ fm gives the

Table IX. Same as Table VIII but for the $R_0 = 1.2$ fm cutoff.

$^Z\text{A} (J^\pi, T)$	Potential	E_C (MeV)	E (MeV)	r_{ch} (fm)
$^6\text{He} (0^+, 1)$	LO	-55.65(6)	-54.9(2)(12.8)	1.31(2)(31)
	NLO	-21.41(6)	-21.8(1)(7.7)	2.08(4)(18)
	N ² LO 2b	-24.25(5)	-24.3(1)(1.8)	2.02(4)(4)
	N ² LO $E\tau$	-28.37(5)	-29.3(1)(1.8)	1.92(4)(4)
	N ² LO $E\mathbb{1}$	-26.98(8)	—	2.00(4)(4)
	exp		-29.3	2.066(11)
$^6\text{Li} (1^+, 0)$	LO	-56.84(3)	-56.0(1)(13.1)	1.59(2)(37)
	NLO	-23.64(8)	-25.2(2)(7.2)	2.47(4)(21)
	N ² LO 2b	-26.76(3)	-27.0(2)(1.7)	2.41(4)(5)
	N ² LO $E\tau$	-30.8(1)	-32.3(3)(1.7)	2.24(4)(6)
	N ² LO $E\mathbb{1}$	-29.0(2)	—	2.27(4)(5)
	exp		-32.0	2.589(39)
$^{16}\text{O} (0^+, 0)$	LO	-1158.8(5)	-1110(31)(259)	1.15(5)(27)
	NLO	-72.3(1)	-77.5(7)(240.8)	2.65(5)(35)
	N ² LO 2b	-98.6(1)	-106(4)(56)	2.47(5)(8)
	N ² LO $E\tau$	-169(2)	-263(26)(56)	2.17(5)(11)
	N ² LO $E\mathbb{1}$	-99.5(4)	-112(8)(56)	2.55(5)(8)
	exp		-127.6	2.669(5)

Table X. Expectation value of the N²LO energy contributions in ^6Li and ^{16}O . All energies (in MeV) are mixed estimates from the constrained evolution: $2 \langle \mathcal{O}_{\text{DMC}} \rangle - \langle \mathcal{O}_{\text{VMC}} \rangle$. Errors are statistical.

System	R_0 (fm)	N ² LO	E_{kin}	v_{ij}	$E_{\text{kin}} + v_{ij}$	V_{ijk}	$V^{2\pi, P}$	$V^{2\pi, S}$	V_D	V_E
^6Li	1.0	2b	116.8(4)	-151.2(4)	-34.4(8)					
	1.0	$E\tau$	135.3(7)	-165.6(5)	-30.2(1.2)	-11.1(3)	-13.3(3)	-0.43(1)	0	2.67(2)
	1.0	$E\mathbb{1}$	135.5(6)	-165.8(6)	-30.3(1.2)	-11.3(2)	-13.3(2)	-0.42(1)	-0.89(2)	3.38(4)
	1.2	2b	110.3(3)	-145.4(3)	-35.1(6)					
	1.2	$E\tau$	129.3(6)	-160.1(5)	-30.8(1.1)	-11.8(3)	-6.1(2)	-0.39(1)	-4.6(1)	-0.63(1)
	1.2	$E\mathbb{1}$	118.0(8)	-153.5(6)	-35.5(1.1)	-5.6(2)	-5.9(2)	-0.25(1)	0.07(3)	0.26(1)
^{16}O	1.0	2b	319(1)	-453(1)	-134(2)					
	1.0	$E\tau$	370(1)	-500(1)	-130(2)	-44(1)	-55(1)	0.85(1)	0	8.50(4)
	1.0	$E\mathbb{1}$	352(1)	-478(1)	-126(2)	-38(1)	-50(1)	0.64(1)	-3.61(3)	14.1(1)
	1.2	2b	377(1)	-528(2)	-151(3)					
	1.2	$E\tau$	556(4)	-712(3)	-156(7)	-202(3)	-101(2)	-0.72(9)	-94(2)	-5.43(3)
	1.2	$E\mathbb{1}$	377(1)	-529(1)	-152(2)	-26(1)	-34(1)	0.93(1)	4.53(8)	1.90(1)

same physical description of the charge form factor as the phenomenological potentials when only one-body charge operators are included.

Two-body densities are related to the Coulomb sum rule, that is defined as the energy integral of the electromagnetic longitudinal response function. As the charge form factor, the Coulomb sum rule can be written as a ground state expectation value [47], leading to the rela-

tion:

$$\begin{aligned}
S_L(q) = & \frac{1}{Z} \frac{1}{G_E^{p,2}(Q_{\text{qe}}^2)} \frac{1}{1 + Q_{\text{qe}}^2/(4m_N^2)} \\
& \times \left\{ G_E^{p,2}(Q_{\text{qe}}^2) [\tilde{\rho}_{pp}(q) + Z] \right. \\
& + G_E^{n,2}(Q_{\text{qe}}^2) [\tilde{\rho}_{nn}(q) + (A - Z)] \\
& + 2 G_E^p(Q_{\text{qe}}^2) G_E^n(Q_{\text{qe}}^2) \tilde{\rho}_{np}(q) \\
& \left. - [G_E^p(Q_{\text{qe}}^2) \tilde{\rho}_p(q) + G_E^n(Q_{\text{qe}}^2) \tilde{\rho}_n(q)]^2 \right\}, \quad (72)
\end{aligned}$$

where $\tilde{\rho}_{\text{NN}}(q)$ is the Fourier transform of the two-body

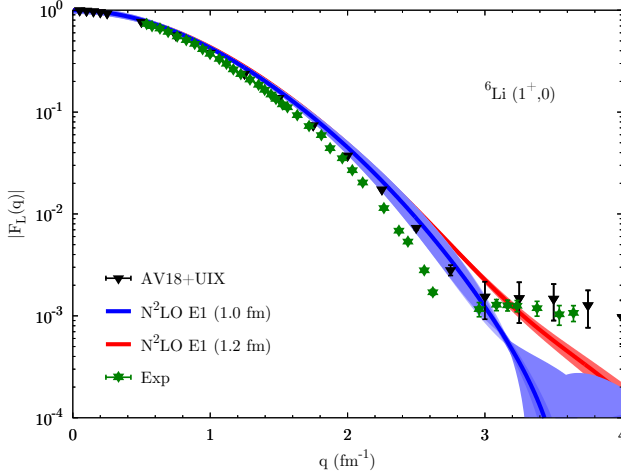


Figure 9. Charge form factor in ${}^6\text{Li}$. The solid blue(red) line is the AFDMC result for the N^2LO $E1$ potential with cutoff $R_0 = 1.0(1.2)$ fm. Lighter shaded areas indicate the uncertainties from the truncation of the chiral expansion. Darker shaded areas are the theoretical error bands only taking into account NLO and N^2LO results. Black triangles are the VMC one-body results for AV18+UIX [49]. The experimental data are taken from Ref. [52].

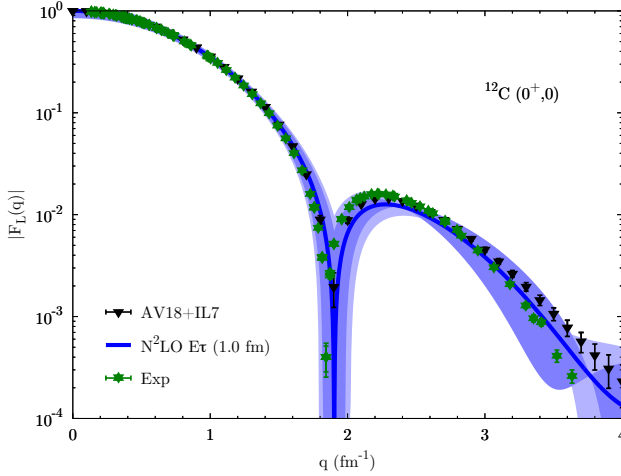


Figure 10. Charge form factor in ${}^{12}\text{C}$. In blue the AFDMC results for the $E\tau$ parametrization of the three-body force and cutoff $R_0 = 1.0$ fm. Black triangles are the GFMC one-body results for AV18+IL7 [50]. The experimental data are taken from Ref. [53]. Updated from Ref. [31].

point-nucleon densities defined in Eq. (70), and $Q_{\text{qe}}^2 = \mathbf{q}^2 - \omega_{\text{qe}}^2$, with ω_{qe} the energy transfer corresponding to the quasielastic peak. Although the Coulomb sum rule is not directly an experimental observable (experimental information can be however extracted from the longitudinal response function, as done in Ref. [58] for ${}^{12}\text{C}$), it is still an interesting observable for the study of integral properties of the response of a nuclear many-body system

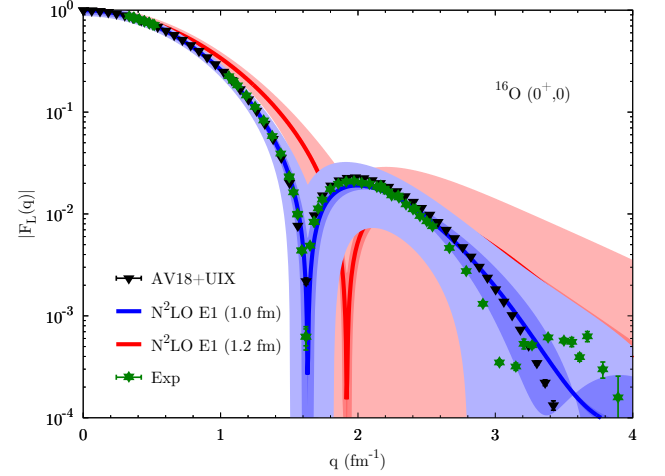


Figure 11. Charge form factor in ${}^{16}\text{O}$. In blue(red) the AFDMC results as in Fig. 9. Black triangles are the cluster-VMC one-body results for AV18+UIX [54]. Experimental data are from I. Sick, based on Refs. [55–57]. Updated from Ref. [31].

to an external probe.

We report in Fig. 12 the Coulomb sum rule for $4 \leq A \leq 16$ using the N^2LO potential with cutoff $R_0 = 1.0$ fm. The GFMC results for ${}^4\text{He}$ and ${}^{12}\text{C}$ [50, 54] employing the AV18+IL7 potential are also shown for comparison. The discrepancy between AFDMC and GFMC above $\approx 3 \text{ fm}^{-1}$ is most likely due to the missing two-body currents in the present calculation. For lower momenta the description of the sum rule is remarkably consistent with that provided by phenomenological potentials. Moreover, the results for ${}^{12}\text{C}$ are compatible with the available experimental data as extracted in Ref. [58], as shown already in [31]. All p -shell nuclei show a similar profile for $S_L(q)$, with a peak around 1.6 fm^{-1} slightly more pronounced for open-shell systems ($A = 6, 12$). The same observations hold for the soft interaction, with the Coulomb sum rule of ${}^4\text{He}$ and ${}^6\text{Li}$ very close to those computed with the hard potential. Exception is the case of ${}^{16}\text{O}$, for which $S_L(q)$ is largely different for the two cutoffs, consistently with the results for the charge form factor, as already shown in Ref. [31].

VII. SUMMARY

The N^2LO potential for $R_0 = 1.0$ fm give a good physical description of nuclei up to ${}^{16}\text{O}$, consistent with experimental data and compatible with that of phenomenological potentials. Softer interactions: discussion to be completed

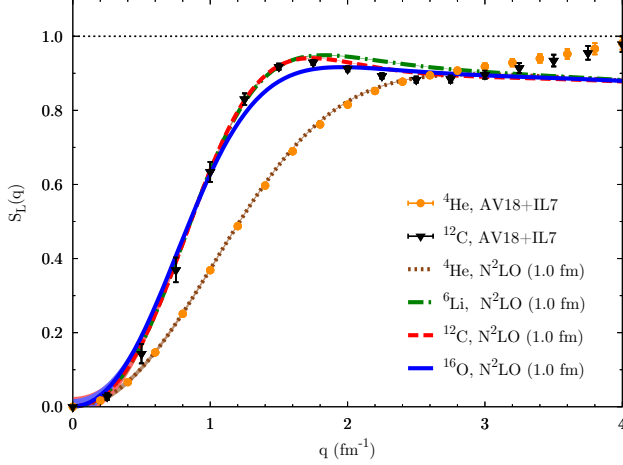


Figure 12. Coulomb sum rule for $4 \leq A \leq 16$. Lines refer to AFDMC results for the $N^2\text{LO } E\tau$ potential with cutoff $R_0 = 1.0\text{ fm}$. Solid symbols are the GFMC one- plus two-body results for AV18+IL7 [50, 54]. Shaded areas indicate the statistical Monte Carlo uncertainty.

ACKNOWLEDGMENTS

We thank I. Tews, A. Lovato, R. F. Garcia Ruiz **ADD OTHERS** for many valuable discussions. The work of D.L. was supported by the U.S. Department of Energy, Office of Science, Office of Nuclear Physics, under the FRIB Theory Alliance Grant Contract No. DE-SC0013617 titled “FRIB Theory Center - A path for the science at FRIB”, and by the NUCLEI SciDAC program. The work of S.G. and J.C. was supported by the NUCLEI SciDAC program, by the U.S. Department of Energy, Office of Science, Office of Nuclear Physics, under contract No. DE-AC52-06NA25396, and by the LDRD program at LANL. K.S. was supported by the National Science Foundation grant PHY-1404405. The work of J.L and A.S. was supported by the ERC Grant No. 307986 STRONGINT and the BMBF under Contract No. 05P15RDFN1. **ADD OTHERS** Computational

resources have been provided by Los Alamos Open Supercomputing via the Institutional Computing (IC) program, and by the National Energy Research Scientific Computing Center (NERSC), which is supported by the U.S. Department of Energy, Office of Science, under contract DE-AC02-05CH11231 **ADD OTHERS**

Appendix A: Calculating two-body correlations

Given $R = \{\mathbf{r}_1, \dots, \mathbf{r}_A\}$ the particle coordinates, $S = \{s_1, \dots, s_A\}$ the spin/isospin configurations, and $|\chi_\gamma\rangle$ the $|p \uparrow\rangle, |p \downarrow\rangle, |n \uparrow\rangle, |n \downarrow\rangle$ basis:

$$\begin{aligned} |\chi_1\rangle &= |(1, 0, 0, 0)\rangle, \\ |\chi_2\rangle &= |(0, 1, 0, 0)\rangle, \\ |\chi_3\rangle &= |(0, 0, 1, 0)\rangle, \\ |\chi_4\rangle &= |(0, 0, 0, 1)\rangle, \end{aligned} \quad (\text{A1})$$

let's define the Slater matrix element

$$S_{\alpha i} = \langle \alpha | \mathbf{r}_i s_i \rangle = \sum_{\gamma=1}^4 \langle \alpha | \mathbf{r}_i \chi_\gamma \rangle \langle \chi_\gamma | s_i \rangle, \quad (\text{A2})$$

where $|\alpha\rangle$ contains the radial orbitals and spherical harmonics of Eq. (59). When acting with two-body correlations on the mean field part of the wave function, the Slater matrix is updated by each of the correlation operators. These updates are computed using the identity

$$\det(S^{-1}S') = \frac{\det S'}{\det S}, \quad (\text{A3})$$

where S' is the matrix that has been updated by the action of a single operator. To reduce the number of operations, the ratio of determinants for a pair of operators, $\mathcal{O}_{ij} = \mathcal{O}_i \mathcal{O}_j$, is written in the form

$$\frac{\langle \Phi | \mathcal{O}_{ij} | RS \rangle}{\langle \Phi | RS \rangle} = \sum_{\gamma=1}^4 \sum_{\delta=1}^4 d_{2b}(\chi_\gamma, \chi_\delta, ij) \langle \chi_\gamma \chi_\delta | \mathcal{O}_{ij} | s_i s_j \rangle, \quad (\text{A4})$$

with

$$d_{2b}(\chi_\gamma, \chi_\delta, ij) = \frac{\langle \Phi | R, s_1, \dots, s_{i-1}, \chi_\gamma, s_{i+1}, \dots, s_{j-1}, \chi_\delta, s_{j+1}, \dots, s_A \rangle}{\langle \Phi | RS \rangle}, \quad (\text{A5})$$

where χ_γ and χ_δ replace s_i and s_j , respectively. The d_{2b} matrix elements are derived from the pre-calculated

matrix elements $P_{\chi, ij}$

$$d_{2b}(\chi_\gamma, \chi_\delta, ij) = \det \begin{pmatrix} P_{\chi_\gamma, ii} & P_{\chi_\gamma, ij} \\ P_{\chi_\delta, ji} & P_{\chi_\delta, jj} \end{pmatrix}, \quad (\text{A6})$$

where

$$\begin{aligned} P_{\chi_\gamma, ij} &= \sum_{\alpha} S_{j\alpha}^{-1} S_{\alpha i} (s_i \leftarrow \chi_\gamma), \\ P_{\chi_\delta, ij} &= \sum_{\alpha} S'_{j\alpha}{}^{-1} S'_{\alpha i} (s_j \leftarrow \chi_\delta). \end{aligned} \quad (\text{A7})$$

Though the above relations only address two-body operators, this method can be generalized to arbitrary N -body operators as well. To include additional operators the matrix elements $P_{\chi, ij}$ need to be updated

$$P_{\chi_\eta, mn} = \sum_{\alpha} S''_{n\alpha}{}^{-1} S''_{\alpha m} (s_m \leftarrow \chi_\eta), \quad (\text{A8})$$

where

$$S''_{\alpha m}(s_m) = \begin{cases} S_{\alpha m} & m \neq i \\ \langle \alpha | \mathcal{O}_i | \mathbf{r}_i s_i \rangle & m = i \end{cases}. \quad (\text{A9})$$

To calculate the updated inverse matrix the identity (A3) is used with $S' \leftarrow S''$. Both sides of the identity are expanded, and like terms are grouped noting that when $j \neq i$, $S''_{mi} = S'_{mi}$.

The wave function with linear correlations (Eq. (55)) is calculated by first acting on the coordinate and spin/isospin configurations with each possible operator, and calculating the sum of each term $\sum_{\chi_\gamma, \chi_\delta} d_{2b}(\chi_\gamma, \chi_\delta, ij) \langle \chi_\gamma, \chi_\delta | f_{ij}^p \mathcal{O}_{ij}^p | s_i s_j \rangle$. The expectation value of the potential on the linear wave function is calculated including correlation and potential operators, \mathcal{O}_{ij}^c and \mathcal{O}_{ij}^p respectively, organized in the form $(1 + \mathcal{O}_{ij}^c) \mathcal{O}_{kl}^p$, that includes four potentially distinct operators. For this calculation the P matrix is updated twice, once for \mathcal{O}_i^c and once for \mathcal{O}_j^c , where $\mathcal{O}_{ij}^c = \mathcal{O}_i^c \mathcal{O}_j^c$

as before. The ratio of determinants is calculated following Eq. (A4), using the updated distribution d''_{2b} .

The quadratic wave function includes the same correlation terms of the linear wave function plus a piece with two additional operators, resulting in structures like $1 + \mathcal{O}_{ij}^c + \mathcal{O}_{ij}^c \mathcal{O}_{kl}^c$. The operators up to linear terms are treated as above. The quadratic product of operators is handled in the same fashion as the expectation value of the potential acting on the linear wave function, i.e., the P matrix is updated twice, once for \mathcal{O}_i^c and once for \mathcal{O}_j^c , and the ratio of determinants is calculated with the updated distributions. It follows that the calculation of the correlation operators for the quadratic wave function requires $o(A^4)$ operations, compared to $o(A^2)$ for the linear wave function.

The expectation value of the potential acting on the quadratic wave function requires the product of six operators $\mathcal{O}_{ij}^c \mathcal{O}_{kl}^c \mathcal{O}_{mn}^p$. As a result, a total of four updates are needed to calculate the quadratically correlated terms for the potential. After including the updated distributions for the \mathcal{O}_{ij}^c operators, the same distributions are updated two more times for the \mathcal{O}_{kl}^c terms. These quadratically updated distributions are then used to calculate the expectation value of the potential as before. It follows that the calculation of the expectation value of the potential acting on the quadratic wave function requires $o(A^6)$ operations, compared to $o(A^4)$ for the linear wave function.

The two-body correlations of Eq. (55) have the same operator structure of the AV6' potential. The cartesian breakup of such structure generates 39 \mathcal{O}_{ij}^c operators, 9 $\sigma_{\alpha i} \sigma_{\beta j}$, 3 $\tau_{\gamma i} \tau_{\gamma j}$, and 27 $\sigma_{\alpha i} \sigma_{\beta j} \tau_{\gamma i} \tau_{\gamma j}$ operators. The number of operators can be reduced to 15 if, instead of cartesian coordinates, one uses the pair distance \mathbf{r}_{ij} and two orthogonal coordinates. This reduces the number of operators used in the spatially dependent part of the tensor term, $3 \sigma_i \cdot \hat{\mathbf{r}}_{ij} \sigma_j \cdot \hat{\mathbf{r}}_{ij}$, from 9 to 3.

-
- [1] J. Carlson, S. Gandolfi, F. Pederiva, S. C. Pieper, R. Schiavilla, K. E. Schmidt, and R. B. Wiringa, *Rev. Mod. Phys.* **87**, 1067 (2015).
 - [2] S. Gandolfi, J. Carlson, and S. C. Pieper, *Phys. Rev. Lett.* **106**, 012501 (2011).
 - [3] S. Gandolfi, J. Carlson, and S. Reddy, *Phys. Rev. C* **85**, 032801 (2012).
 - [4] P. Maris, J. P. Vary, S. Gandolfi, J. Carlson, and S. C. Pieper, *Phys. Rev. C* **87**, 054318 (2013).
 - [5] S. Gandolfi, A. Lovato, J. Carlson, and K. E. Schmidt, *Phys. Rev. C* **90**, 061306 (2014).
 - [6] S. Gandolfi, J. Carlson, S. Reddy, A. W. Steiner, and R. B. Wiringa, *Eur. Phys. J. A* **50**, 10 (2014).
 - [7] M. Buraczynski and A. Gezerlis, *Phys. Rev. Lett.* **116**, 152501 (2016).
 - [8] M. Buraczynski and A. Gezerlis, *Phys. Rev. C* **95**, 044309 (2017).
 - [9] A. Sarsa, S. Fantoni, K. E. Schmidt, and F. Pederiva, *Phys. Rev. C* **68**, 024308 (2003).
 - [10] P. B. Demorest, T. Pennucci, S. M. Ransom, M. S. E. Roberts, and J. W. T. Hessels, *Nature* **467**, 1081 (2010).
 - [11] J. Antoniadis, P. C. C. Freire, N. Wex, T. M. Tauris, R. S. Lynch, M. H. van Kerkwijk, M. Kramer, C. Bassa, V. S. Dhillon, T. Driebe, J. W. T. Hessels, V. M. Kaspi, V. I. Kondratiev, N. Langer, T. R. Marsh, *et al.*, *Science* **340**, 6131 (2013).
 - [12] E. Epelbaum, H.-W. Hammer, and U.-G. Meißner, *Rev. Mod. Phys.* **81**, 1773 (2009).
 - [13] R. Machleidt and D. R. Entem, *Phys. Rep.* **503**, 1 (2011).
 - [14] A. Ekström, G. Baardsen, C. Forssén, G. Hagen, M. Hjorth-Jensen, G. R. Jansen, R. Machleidt, W. Nazarewicz, T. Papenbrock, J. Sarich, and S. M. Wild, *Phys. Rev. Lett.* **110**, 192502 (2013).
 - [15] D. R. Entem, N. Kaiser, R. Machleidt, and Y. Nosyk, *Phys. Rev. C* **91**, 014002 (2015).
 - [16] E. Epelbaum, H. Krebs, and U.-G. Meißner, *Phys. Rev. Lett.* **115**, 122301 (2015).
 - [17] A. Ekström, G. R. Jansen, K. A. Wendt, G. Hagen, T. Papenbrock, B. D. Carlsson, C. Forssén, M. Hjorth-Jensen, P. Navrátil, and W. Nazarewicz, *Phys. Rev. C*

- 91**, 051301 (2015).
- [18] A. Ekström, G. Hagen, T. D. Morris, T. Papenbrock, and P. D. Schwartz, [arXiv:1707.09028](#).
 - [19] A. Gezerlis, I. Tews, E. Epelbaum, S. Gandolfi, K. Hebeler, A. Nogga, and A. Schwenk, *Phys. Rev. Lett.* **111**, 032501 (2013).
 - [20] A. Gezerlis, I. Tews, E. Epelbaum, M. Freunek, S. Gandolfi, K. Hebeler, A. Nogga, and A. Schwenk, *Phys. Rev. C* **90**, 054323 (2014).
 - [21] I. Tews, S. Gandolfi, A. Gezerlis, and A. Schwenk, *Phys. Rev. C* **93**, 024305 (2016).
 - [22] J. E. Lynn, I. Tews, J. Carlson, S. Gandolfi, A. Gezerlis, K. E. Schmidt, and A. Schwenk, *Phys. Rev. Lett.* **116**, 062501 (2016).
 - [23] M. Piarulli, L. Girlanda, R. Schiavilla, R. Navarro Pérez, J. E. Amaro, and E. Ruiz Arriola, *Phys. Rev. C* **91**, 024003 (2015).
 - [24] M. Piarulli, L. Girlanda, R. Schiavilla, A. Kievsky, A. Lovato, L. E. Marcucci, S. C. Pieper, M. Viviani, and R. B. Wiringa, *Phys. Rev. C* **94**, 054007 (2016).
 - [25] M. Piarulli, A. Baroni, L. Girlanda, A. Kievsky, A. Lovato, E. Lusk, L. E. Marcucci, S. C. Pieper, R. Schiavilla, M. Viviani, and R. B. Wiringa, [arXiv:1707.02883](#).
 - [26] J. E. Lynn, I. Tews, J. Carlson, S. Gandolfi, A. Gezerlis, K. E. Schmidt, and A. Schwenk, *Phys. Rev. C* **96**, 054007 (2017).
 - [27] J. E. Lynn, J. Carlson, E. Epelbaum, S. Gandolfi, A. Gezerlis, and A. Schwenk, *Phys. Rev. Lett.* **113**, 192501 (2014).
 - [28] P. Klos, J. E. Lynn, I. Tews, S. Gandolfi, A. Gezerlis, H.-W. Hammer, M. Hoferichter, and A. Schwenk, *Phys. Rev. C* **94**, 054005 (2016).
 - [29] P. W. Zhao and S. Gandolfi, *Phys. Rev. C* **94**, 041302 (2016).
 - [30] S. Gandolfi, H.-W. Hammer, P. Klos, J. E. Lynn, and A. Schwenk, *Phys. Rev. Lett.* **118**, 232501 (2017).
 - [31] D. Lonardoni, J. Carlson, S. Gandolfi, J. E. Lynn, K. E. Schmidt, A. Schwenk, and X. Wang, [arXiv:1709.09143 \[nucl-th\]](#).
 - [32] R. Wiringa and S. Pieper, *Phys. Rev. Lett.* **89**, 18 (2002).
 - [33] N. Metropolis, A. W. Rosenbluth, M. N. Rosenbluth, A. H. Teller, and E. Teller, *J. Chem. Phys.* **21**, 1087 (1953).
 - [34] D. M. Ceperley, *Rev. Mod. Phys.* **67**, 279 (1995).
 - [35] S. C. Pieper, “Monte carlo calculations of nuclei,” in *Microscopic Quantum Many-Body Theories and Their Applications: Proceedings of a European Summer School Held at Valencia, Spain, 8-19 September 1997*, edited by J. Navarro and A. Polls (Springer Berlin Heidelberg, Berlin, Heidelberg, 1998) pp. 337–357.
 - [36] B. S. Pudliner, V. R. Pandharipande, J. Carlson, S. C. Pieper, and R. B. Wiringa, *Phys. Rev. C* **56**, 1720 (1997).
 - [37] W. M. C. Foulkes, L. Mitas, R. J. Needs, and G. Rajagopal, *Rev. Mod. Phys.* **73**, 33 (2001).
 - [38] M. Pervin, S. C. Pieper, and R. B. Wiringa, *Phys. Rev. C* **76**, 064319 (2007).
 - [39] S. Zhang and H. Krakauer, *Phys. Rev. Lett.* **90**, 136401 (2003).
 - [40] S. Zhang, J. Carlson, and J. E. Gubernatis, *Phys. Rev. B* **55**, 7464 (1997).
 - [41] G. Ortiz, D. M. Ceperley, and R. M. Martin, *Phys. Rev. Lett.* **71**, 2777 (1993).
 - [42] E. Epelbaum, H. Krebs, and U.-G. Meißner, *Eur. Phys. J. A* **51**, 53 (2015).
 - [43] J. Beringer, J. F. Arguin, R. M. Barnett, K. Copic, O. Dahl, D. E. Groom, C. J. Lin, J. Lys, H. Murayama, C. G. Wohl, W. M. Yao, P. A. Zyla, C. Amsler, M. Antonelli, D. M. Asner, *et al.* (Particle Data Group), *Phys. Rev. D* **86**, 010001 (2012).
 - [44] J. L. Friar, J. Martorell, and D. W. L. Sprung, *Phys. Rev. A* **56**, 4579 (1997).
 - [45] A. Ong, J. C. Berengut, and V. V. Flambaum, *Phys. Rev. C* **82**, 014320 (2010).
 - [46] I. Angeli and K. Marinova, *Atomic Data and Nuclear Data Tables* **99**, 69 (2013).
 - [47] K. W. McVoy and L. Van Hove, *Phys. Rev.* **125**, 1034 (1962).
 - [48] J. J. Kelly, *Phys. Rev. C* **70**, 068202 (2004).
 - [49] R. B. Wiringa and R. Schiavilla, *Phys. Rev. Lett.* **81**, 4317 (1998).
 - [50] A. Lovato, S. Gandolfi, R. Butler, J. Carlson, E. Lusk, S. C. Pieper, and R. Schiavilla, *Phys. Rev. Lett.* **111**, 092501 (2013).
 - [51] B. Mihaila and J. H. Heisenberg, *Phys. Rev. Lett.* **84**, 1403 (2000).
 - [52] G. C. Li, I. Sick, R. R. Whitney, and M. R. Yearian, *Nucl. Phys. A* **162**, 583 (1971).
 - [53] H. De Vries, C. W. De Jager, and C. De Vries, *At. Data Nucl. Data Tables* **36**, 495 (1987).
 - [54] D. Lonardoni, A. Lovato, S. C. Pieper, and R. B. Wiringa, *Phys. Rev. C* **96**, 024326 (2017).
 - [55] I. Sick and J. S. McCarthy, *Nucl. Phys. A* **150**, 631 (1970).
 - [56] W. Schuetz, *Z Phys. A* **273**, 69 (1975).
 - [57] I. Sick, (unpublished).
 - [58] A. Lovato, S. Gandolfi, J. Carlson, S. C. Pieper, and R. Schiavilla, *Phys. Rev. Lett.* **117**, 082501 (2016).